

# 1    **First real-time isotopic characterisation of N<sub>2</sub>O from chemodenitrification**

2    Jing Wei <sup>a,b,\*</sup>, Erkan Ibraim <sup>b</sup>, Nicolas Brüggemann <sup>a</sup>, Harry Vereecken <sup>a</sup>, Joachim Mohn <sup>b</sup>

3  
4    <sup>a</sup>*Forschungszentrum Jülich GmbH, Institute of Bio- and Geosciences, Agrosphere (IBG-3), Wilhelm-*  
5    *Johnen-Straße, 52425 Jülich, Germany*

6    <sup>b</sup>*Empa, Swiss Federal Laboratories for Materials Science and Technology, Laboratory for Air Pollution*  
7    *& Environmental Technology, Überlandstrasse 129, 8600 Dübendorf, Switzerland*

8    \* Corresponding author: E-mail address, [jing.wei@empa.ch](mailto:jing.wei@empa.ch) (J. Wei); Tel.: +41 58 765 4512; Fax: +41  
9    58 765 1122

This document is the accepted manuscript version of the following article:

Wei, J., Ibraim, E., Brüggemann, N., Vereecken, H., & Mohn, J. (2019). First real-time isotopic characterisation of N<sub>2</sub>O from chemodenitrification. *Geochimica et Cosmochimica Acta*, 267, 17-32. <https://doi.org/10.1016/j.gca.2019.09.018>

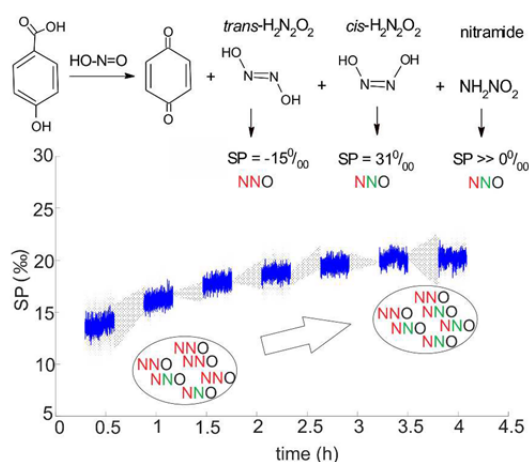
This manuscript version is made available under the CC-BY-NC-ND 4.0 license <http://creativecommons.org/licenses/by-nc-nd/4.0/>

## Abstract

Chemodenitrification can be a substantial abiotic source of nitrous oxide ( $\text{N}_2\text{O}$ ) in soil. The isotopic signature of  $\text{N}_2\text{O}$  from this process could support source partitioning, but it is currently unknown in sufficient detail. In this study, we determined the isotopic composition of  $\text{N}_2\text{O}$ , produced by the reaction of nitrite ( $\text{NO}_2^-$ ) with lignin, four lignin derivatives, and three types of soils, online with a quantum cascade laser absorption spectrometer (QCLAS). We present the first dataset of continuous measurements of  $\delta^{15}\text{N}^{\text{bulk}}$  ( $\delta^{15}\text{N}^{\text{bulk}} \equiv (\delta^{15}\text{N}^{\alpha} + \delta^{15}\text{N}^{\beta})/2$ ),  $\delta^{18}\text{O}$ , and site preference ( $\text{SP}_{\text{N}_2\text{O}}$ ,  $\text{SP}_{\text{N}_2\text{O}} \equiv \delta^{15}\text{N}^{\alpha} - \delta^{15}\text{N}^{\beta}$ ) of  $\text{N}_2\text{O}$  from chemodenitrification in both chemical assays and soils. Considerable amounts of  $\text{N}_2\text{O}$  were produced by chemical reduction of  $\text{NO}_2^-$ , indicating that chemodenitrification could dominate  $\text{N}_2\text{O}$  emission in  $\text{NO}_2^-$ -rich environments. The values of  $\text{SP}_{\text{N}_2\text{O}}$  varied by more than 20‰ in the reactions of sodium nitrite with organic substances. Contrary to the common assumption that  $\text{SP}_{\text{N}_2\text{O}}$  values are constant for a distinct  $\text{N}_2\text{O}$  source process, our results reveal a considerable shift in  $\text{SP}_{\text{N}_2\text{O}}$  over time for most experiments. The large  $\text{SP}_{\text{N}_2\text{O}}$  variability might be explained by the multiple pathways with hyponitrous acid or nitramide as  $\text{N}_2\text{O}$  precursors. These findings provide important new information to improve our understanding about the dependency of  $\text{N}_2\text{O}$  isotopic signatures on  $\text{N}_2\text{O}$  production processes.

**Keywords:** Chemodenitrification; Nitrous oxide; Site preference; Nitrite; Lignin derivatives

## TOC Art



## 1. INTRODUCTION

Nitrous oxide ( $\text{N}_2\text{O}$ ), whose radiative efficiency in the troposphere is almost 300-fold higher than that of carbon dioxide, is the third most important long-lived greenhouse gas contributing about 6% to total anthropogenic global warming (IPCC, 2013). Furthermore,  $\text{N}_2\text{O}$  can decompose to nitric oxide ( $\text{NO}$ ), which further reduces ozone to oxygen, through photolysis in the stratosphere, hence  $\text{N}_2\text{O}$  is also contributing to the depletion of the ozone layer (Ravishankara et al., 2009). After successful emission reduction of chlorine- and bromine-containing halocarbons supported by the Montreal protocol,  $\text{N}_2\text{O}$  currently represents the single most important ozone-depleting substance and it is likely to remain the largest one in the 21<sup>st</sup> century (Ravishankara et al., 2009). However, the  $\text{N}_2\text{O}$  global mixing ratio has increased by 21% up until 2015 (328 ppb) compared with the pre-industrial level and is still increasing by around  $0.89 \text{ ppb yr}^{-1}$ , mainly due to the use of nitrogen fertiliser in agriculture (WMO, 2016). Therefore, it is currently imperative to mitigate global  $\text{N}_2\text{O}$  emissions, which would require a better understanding of relevant  $\text{N}_2\text{O}$  production pathways.

For a long period of time, microbial nitrification and denitrification conducted by bacteria, fungi and archaea have been considered as the main  $\text{N}_2\text{O}$  source processes. During nitrification, ammonium ( $\text{NH}_4^+$ ) is first oxidised to hydroxylamine ( $\text{NH}_2\text{OH}$ ) by ammonium oxidisers, which is afterwards oxidised to nitrite ( $\text{NO}_2^-$ ) under the catalyst of hydroxylamine oxidoreductase (HAO), while  $\text{N}_2\text{O}$  is released as a byproduct of either biotic or abiotic  $\text{NH}_2\text{OH}$  oxidation (Caranto and Lancaster, 2017; Liu et al., 2017; Stein, 2011). In the case of denitrification including bacterial, fungal, and nitrifier denitrification,  $\text{N}_2\text{O}$  is considered as an obligatory intermediate or end product of biotic reduction of  $\text{NO}_2^-$  (Stein, 2011; Sutka et al., 2008). However,  $\text{NO}_2^-$  can be released through both nitrification and denitrification into the soil and rapidly chemically reduced to  $\text{N}_2\text{O}$  by soil organic matter (SOM) or transition metals, which is termed as chemodenitrification (Chalk and Smith, 1983). Acidic conditions largely promote chemodenitrification processes because the chemical reactivity of nitrous acid ( $\text{HNO}_2$ ), formed through the protonation of  $\text{NO}_2^-$ , is much higher than that of the  $\text{NO}_2^-$  ion itself (Chalk and Smith, 1983). Increasing evidence demonstrates that  $\text{N}_2\text{O}$  emission from

chemodenitrification can be substantial in various ecosystems, including extreme arid and cold lakes, ponds, and soils (Ostrom et al., 2016; Peters et al., 2014; Samarkin et al., 2010), temperate forests and arable lands (Venterea, 2007; Wei et al., 2017a), and sediments (Wankel et al., 2017). Therefore, the contribution of chemodenitrification to global N<sub>2</sub>O emissions could have been largely underestimated.

Stable isotope techniques offer a powerful tool to disentangle N<sub>2</sub>O production pathways in the environment. Since the two nitrogen atoms are located asymmetrically in the linear N<sub>2</sub>O molecule (N<sup>β</sup>N<sup>α</sup>O), the difference of δ<sup>15</sup>N between the α and β position is defined as site preference (SP<sub>N<sub>2</sub>O</sub> ≡ δ<sup>15</sup>N<sup>α</sup> – δ<sup>15</sup>N<sup>β</sup>) (Toyoda and Yoshida, 1999). Independent of the isotopic composition of the substrates, SP<sub>N<sub>2</sub>O</sub> has been thought to be very specific for a certain N<sub>2</sub>O production pathway and represents the transient state of the N<sub>2</sub>O formation and reduction (Toyoda and Yoshida, 1999; Toyoda et al., 2002). Microbial N<sub>2</sub>O sources of nitrification and fungal denitrification, as well as chemical oxidation of NH<sub>2</sub>OH, feature relatively high SP<sub>N<sub>2</sub>O</sub> values of 27 - 40‰ (Heil et al., 2014; Heil et al., 2015; Rohe et al., 2014; Sutka et al., 2003; Sutka et al., 2006; Sutka et al., 2008; Toyoda et al., 2005), while bacterial denitrification and nitrifier denitrification are characterised by low SP<sub>N<sub>2</sub>O</sub> values of -11 to 1.4‰ (Frame and Casciotti, 2010; Sutka et al., 2003; Sutka et al., 2006; Toyoda et al., 2005). The reduction of N<sub>2</sub>O to N<sub>2</sub> by heterotrophic denitrifiers is characterised by an isotopic enrichment factor for SP<sub>N<sub>2</sub>O</sub> of -5.0 to -6.8‰ (Lewicka-Szczebak et al., 2017; Ostrom et al., 2007).

The δ<sup>15</sup>N<sup>bulk</sup> values of N<sub>2</sub>O are highly influenced by the isotope effects of both N<sub>2</sub>O production and reduction. During nitrification, the <sup>15</sup>N in N<sub>2</sub>O is enriched by -0.3–5.7‰ for NH<sub>2</sub>OH oxidation (Sutka et al., 2003; Sutka et al., 2006), but depleted by 18.6–68‰ and 12.3–34.3‰ for NH<sub>4</sub><sup>+</sup> oxidation by ammonia oxidizing bacteria (AOB) and ammonia oxidizing archaea (AOA), respectively (Frame and Casciotti, 2010; Jung et al., 2014; Mandernack et al., 2009; Yamazaki et al., 2014). In contrast, N<sub>2</sub>O is <sup>15</sup>N-depleted by 10–37‰ and 30.9–45.6‰ during nitrate (NO<sub>3</sub><sup>-</sup>) reduction by denitrifying bacteria and fungi, respectively (Rohe et al., 2014; Sutka et al., 2006; Toyoda et al., 2005). When NO<sub>2</sub><sup>-</sup> is reduced to N<sub>2</sub>O, N<sub>2</sub>O is <sup>15</sup>N-depleted by 31.4–39.5‰ for nitrifier denitrification and by

8.5–29.0‰ for fungal denitrification (Rohe et al., 2014; Sutka et al., 2003; Sutka et al., 2008; Yoshida, 1988). In addition, the reduction of  $\text{N}_2\text{O}$  to  $\text{N}_2$  by heterotrophic denitrifiers is accompanied by a 4.1–6.6‰ decrease in  $\delta^{15}\text{N}$  due to the isotope effect of N-O bond cleavage (Lewicka-Szczebak et al., 2017; Ostrom et al., 2007).

Despite the depletion of  $^{15}\text{N}$ ,  $^{18}\text{O}$  is generally enriched in  $\text{N}_2\text{O}$  by 3–12.6‰ for nitrification (Jung et al., 2014; Santoro et al., 2011), and by 4–23‰ and 13.2–33.3‰ for  $\text{NO}_3^-$  reduction to  $\text{N}_2\text{O}$  by denitrifying bacteria and fungi, respectively (Rohe et al., 2014; Toyoda et al., 2005).  $^{18}\text{O}$  enrichment of  $\text{N}_2\text{O}$  ranges from 34.2 to 60.8‰ for  $\text{NO}_2^-$  reduction during fungal denitrification and was found to be 8.4‰ during nitrifier denitrification (Frame and Casciotti, 2010; Rohe et al., 2014). The O exchange of reaction intermediates with water is a key factor affecting the fractionation effect of  $^{18}\text{O}$  (Kool et al., 2007; Kool et al., 2009; Kool et al., 2011). Significant differences in  $^{18}\text{O}$  exchange were observed between bacterial and fungal denitrification (Lewicka-Szczebak et al., 2016), varying from 17 to 94% depending on the  $\text{N}_2\text{O}$  production pathways and environmental conditions (Rohe et al., 2017). Based on the above-mentioned results,  $\text{N}_2\text{O}$  isotopic signatures have been widely used to partition  $\text{N}_2\text{O}$  sources for wastewater treatment systems (Harris et al., 2015; Wunderlin et al., 2013) and natural ecosystems from local (Bol et al., 2003; Toyoda et al., 2009; Toyoda et al., 2011; Wolf et al., 2015) to global scales (Röckmann and Levin, 2005; Snider et al., 2015; Toyoda et al., 2013).

In spite of the fact that chemodenitrification accounts for substantial  $\text{N}_2\text{O}$  emissions in certain ecosystems, its  $\text{N}_2\text{O}$  isotopic signature has not been investigated in sufficient detail (Ostrom et al., 2016; Zhu-Barker et al., 2015). Moreover, the currently reported  $\text{N}_2\text{O}$  isotopic signatures of chemodenitrification are discordant with each other for varying reaction conditions. The reported  $\text{SP}_{\text{N}_2\text{O}}$  values include: 10 to 22‰ for the abiotic reduction of  $\text{NO}_2^-$  by ferrous iron ( $\text{Fe}^{2+}$ ) at neutral pH when oxygen is limiting (Jones et al., 2015), 20 to 26‰ for the chemical reaction of  $\text{NO}_2^-$  with SOM at pH 3.8 (Wei et al., 2017a), around 30‰ for the reaction of  $\text{NO}_2^-$  with trimethylamine-borane at pH 1 (Toyoda et al., 2005), and 34 to 35‰ for the chemical reaction of  $\text{NH}_2\text{OH}$  with  $\text{NO}_2^-$  at pH 3–6 (Heil et

al., 2014). Thus, more sophisticated studies are needed to explain this large variability, as well as to evaluate its use for N<sub>2</sub>O source attribution.

Lignin is a phenolic polymer accounting for 20% of organic carbon in the terrestrial biosphere, and its degradation in soil produces various phenolic compounds which are chemically highly reactive to NO<sub>2</sub><sup>-</sup> (Thevenot et al., 2010). It has been reported that the NO<sub>2</sub><sup>-</sup> related N<sub>2</sub>O emission is positively correlated to the lignin content in acidic organic-rich forest soils (Wei et al., 2017a). Therefore, the reaction of lignin and its derivatives with NO<sub>2</sub><sup>-</sup> might play a key role in chemodenitrification. A previous study showed that the SP<sub>N<sub>2</sub>O</sub> of abiotic reactions of NO<sub>2</sub><sup>-</sup> with lignin derivatives varied largely depending on pH and lignin-derived reactants (Wei et al., 2017b). The question of whether SP<sub>N<sub>2</sub>O</sub> remain constant during NO<sub>2</sub><sup>-</sup> reduction by SOM is vital for a process-level understanding and interpretation of potential reaction mechanisms. To answer this question, we investigated the N<sub>2</sub>O isotopic signatures from reactions of NO<sub>2</sub><sup>-</sup> with five lignin-derived compounds in real time, as well as NO<sub>2</sub><sup>-</sup>-related N<sub>2</sub>O emissions in three types of soils for the first time by laser spectroscopy. In addition to N<sub>2</sub>O, other by-products of the reaction, i.e. NO and phenols, were investigated with chemiluminescence and gas chromatography-mass spectrometry, respectively, to further elucidate the reaction mechanisms.

## 2. MATERIALS AND METHODS

### 2.1. Laser spectroscopic analysis of N<sub>2</sub>O isotopic composition

The analyser used in this study was a commercially available quantum cascade laser absorption spectrometer (QCLAS, CW-QC-TILDAS-76-CS; Aerodyne Research Inc., Billerica, USA) that has been customised for simultaneous analysis of the four most abundant N<sub>2</sub>O isotopic species, i.e. <sup>14</sup>N<sup>14</sup>N<sup>16</sup>O, <sup>14</sup>N<sup>15</sup>N<sup>16</sup>O, <sup>15</sup>N<sup>14</sup>N<sup>16</sup>O, and <sup>14</sup>N<sup>14</sup>N<sup>18</sup>O (Ibraim et al., 2018). The QCLAS comprises a continuous-wave mid-infrared quantum cascade laser source (Alpes Lasers SA, Switzerland) emitting at 2203 cm<sup>-1</sup> and an astigmatic multi-pass absorption cell with a path length of 76 m and a cell volume of 0.62 L. Laser control, data acquisition, and quantification of the N<sub>2</sub>O isotopic species are performed using TDL

Wintel (Aerodyne Research Inc., Billerica, USA). The QCLAS was operated in a flow-through mode with a temporal resolution of 1 Hz for data acquisition. The Allan variance precision of the spectrometer for ratios of isotopic species  $R^\alpha$ ,  $R^\beta$ , and  $R^{18\text{O}}$  with 1250 s spectral averaging was less than 0.1‰ (1  $\sigma$  standard deviation) (Werle et al., 1993). The gas flow through the QCLAS gas cell was adjusted to 12 mL min<sup>-1</sup> and the cell pressure was kept at  $26.67 \pm 0.01$  hPa using a pressure controller (MKS Instruments, Andover, MA, USA).

The isotope ratios of samples were corrected using a two-point calibration approach with calibration gas 1 (Cal1,  $\delta^{15}\text{N}^\alpha = -22.21 \pm 0.39\text{‰}$  vs. air-N<sub>2</sub>,  $\delta^{15}\text{N}^\beta = -49.28 \pm 0.40\text{‰}$  vs. air-N<sub>2</sub>,  $\delta^{18}\text{O} = 26.94 \pm 0.23\text{‰}$  vs. VSMOW) and calibration gas 2 (Cal2,  $\delta^{15}\text{N}^\alpha = -0.13 \pm 0.28\text{‰}$  vs. air-N<sub>2</sub>,  $\delta^{15}\text{N}^\beta = 1.35 \pm 0.29\text{‰}$  vs. air-N<sub>2</sub>,  $\delta^{18}\text{O} = 38.46 \pm 0.15\text{‰}$  vs. VSMOW) at 36 ppm. Both Cal1 and Cal2 were prepared in synthetic air (20.5% of O<sub>2</sub>, 79.5% of N<sub>2</sub>, 99.999% purity, Messer Schweiz AG, Switzerland) as described in Waechter et al. (2008) and calibrated against standard gases which were primarily analysed by Sakae Toyoda at Tokyo Institute of Technology (Mohn et al., 2014; Toyoda and Yoshida, 1999). To account for drift effects of the QCLAS, Cal1, diluted to 35 ppm N<sub>2</sub>O, was analysed at least every 35 min for 10 min. Nonlinearity effects of N<sub>2</sub>O concentration on isotope ratios were determined, before and after each experiment, analysing Cal1 at 12, 25, 36, 45, 54, 68, 82 ppm N<sub>2</sub>O and corrected as described below. The selection of sample versus calibration gas was conducted by two 3-way solenoid valves (series 9, Parker Hannifin, USA).

## 2.2. Experimental setup

The experimental setup for online measurement of N<sub>2</sub>O isotopocules is illustrated in Fig. 1. A quartz glass chamber with a PTFE cover plate was used as the reaction chamber. To decrease the delay time and increase the real-time response of the system, the volume of the reaction chamber was reduced to 300 mL by inserting a hollow polypropylene cylinder. In addition, a fan was installed at the top of the chamber to ensure that the headspace gas phase was homogeneously mixed. The absence of significant leaks (pressure drop < 100 Pa min<sup>-1</sup> at 0.1 MPa overpressure) was assured with

a leak test before every experiment. Gas flows in the setup were controlled using mass flow controllers (MFCs, Redy Smart series, Vögtlin Instruments, Switzerland) and a number of two- and three-position solenoid valves (Parker Hannifin Corp., USA). The experimental setup was controlled via a custom-written LabVIEW code (National Instruments Corp., USA), and devices were connected via a 16-port serial-to-ethernet network connector (Etherlite 160, Digi International Inc., USA).

The reactor was continuously purged with 14–16 mL min<sup>-1</sup> of synthetic air (20.5% of O<sub>2</sub>, 79.5% of N<sub>2</sub>, 99.999% purity, Messer Schweiz AG, Switzerland) to deliver the liberated process gases into the spectrometer gas cell. The sample gas was dehumidified using a Nafion permeation dryer (MD-050-72S-1, Perma Pure, USA) and the overflow which was not subjected to laser spectroscopic analysis was exhausted into a fume hood, thereby keeping the pressure of the reaction chamber constant at ambient pressure. Carbon monoxide (CO) was removed with a Sofnocat oxidation catalyst (Sofnocat 423, Molecular Products Ltd., United Kingdom), as CO would otherwise induce spectral interferences during QCLAS analysis. Thereafter, carbon dioxide (CO<sub>2</sub>) was removed from the process gas with a trap containing 13.8 g of ascarite (10–35 mesh, Fluka, Switzerland) bracketed with magnesium perchlorate (Mg(ClO<sub>4</sub>)<sub>2</sub>, 2 × 3.5 g, Fluka, Switzerland) and separated with glass wool (BGB Analytics AG, Switzerland). If N<sub>2</sub>O concentrations in the sample gas were above 82 ppm, the gas was diluted by adding an additional flow of synthetic air through MFC1 and the N<sub>2</sub>O concentration in the undiluted process gas was back-calculated by multiplying the measured N<sub>2</sub>O concentration with the dilution factor. Since co-production of nitric oxide (NO) was expected together with N<sub>2</sub>O, the absence of spectral interferences by NO was assured by a pre-test, where 50 ppm NO was added to a N<sub>2</sub>O calibration gas and no significant change in the analysed N<sub>2</sub>O isotopic composition was observed.

### 2.3. Experimental procedure

Sodium nitrite (NaNO<sub>2</sub>, VWR, Germany) was used as the NO<sub>2</sub><sup>-</sup> source, and its δ<sup>15</sup>N (-18.00 ± 0.08‰ vs. air-N<sub>2</sub>) and δ<sup>18</sup>O (10.09 ± 0.05‰ vs. VSMOW) were measured using an elemental analyser coupled to an isotope ratio mass spectrometer (EA-IRMS, Flash EA 2000 and Delta V Plus; Thermo Fisher



Scientific, Bremen, Germany). Common lignin-derived compounds, organosolv lignin (Chemical Point UG, Oberhaching, Germany), 4-hydroxybenzoic acid, 4-hydroxy-3-methoxybenzoic acid, 4-hydroxy-3,5-dimethoxybenzoic acid, and 4-hydroxy-3,5-dimethoxybenzaldehyde (VWR, Germany) (Wei et al., 2017b), were chosen as model substances in this study. All chemicals were reagent grade or better. Forest and grassland soils were sampled from the O<sub>a</sub> layer of the Wüstebach catchment (50°30'15"N, 6°18'15"E) and the Rollesbroich grassland (50°37'0"N, 6°26'0"E), respectively, in the northern Eifel region, Germany. The sites are part of the German environmental monitoring programme, named TERENO (Zacharias et al., 2011). Agricultural soil was sampled from the top layer (0–20 cm) of the Hohenschulen experimental farm (54°19'05"N, 9°58'38"E) at the University of Kiel, Germany. The characteristics of all soils are listed in Table 1.

A 100-mL beaker containing 5–26 g of carbon substances or soil together with a stir bar was placed into the chamber. Then, the whole setup was flushed using 18 mL min<sup>-1</sup> of synthetic air until the N<sub>2</sub>O concentration declined and stabilised at < 0.1 ppm. Afterwards, 50 mL of NaNO<sub>2</sub> solution in ultrapure water (18.2 MΩ cm) was injected into the beaker through a rubber septum on top of the chamber. A magnetic stirrer was used to mix the reactants for 5 min. Experimental details for each treatment including the amount of carbon substances/soils and NaNO<sub>2</sub> and flow rate of the carrier gas are listed in Table 2. Different substrate-to-nitrite ratios were chosen to reach the calibrated N<sub>2</sub>O concentration range (12–82 ppm), and higher N<sub>2</sub>O mixing ratios (>80 ppm) were diluted by manually adding a dilution flow of synthetic air. For sterilisation treatments, soils were distributed in portions of 10 g each into 50 mL glass bottles with screw caps (VWR, Germany) and autoclaved for 30 min at 1.2 bar and 121°C, and NaNO<sub>2</sub> solution and carrier gas were passed through a 0.2 µm PTFE filter. The online measurements of N<sub>2</sub>O isotopic signatures lasted for 4–6 h, and all experiments were conducted in triplicate. pH was measured at an interval of 25–90 min using a pH meter (model 720, Orion Research, Inc., Jacksonville, Florida, USA).

## 2.4. Analysis of N<sub>2</sub>O and NO<sub>x</sub> emissions and organic reaction products

In a separate set of experiments, N<sub>2</sub>O and nitrogen oxide (NO<sub>x</sub>) emissions were analysed by a combination of a dual quantum cascade laser absorption spectrometer (QCLAS, DUAL CW RT-QC-TILDAS-76, Aerodyne Research, Inc., Billerica, MA, USA) and a chemiluminescence based analyser (CLD, AC32M, Ansyco GmbH, Karlsruhe, Germany). In each experiment, 0.5 g of lignin or 0.3 mmol of lignin derivatives was placed into a 100 mL beaker in a reaction chamber of 2 L volume. The system was purged with 3 L min<sup>-1</sup> of synthetic air (20.5% oxygen and 79.5% nitrogen) until N<sub>2</sub>O and NO<sub>x</sub> signals decreased to below 0.1 and 0.01 ppb, respectively. Then, 100 mL of 1 mM sodium nitrite (VWR, Germany) solution was injected into the reaction beaker and the mixing ratios of NO<sub>x</sub> and N<sub>2</sub>O were recorded with temporal resolution of 5 s and 1 s, respectively.

The organic products of the reactions of NO<sub>2</sub><sup>-</sup> with 4-hydroxy-3-methoxybenzoic acid, 4-hydroxy-3,5-dimethoxybenzoic acid, and lignin were determined using a gas chromatography-mass spectrometry (GC-MS). In detail, 0.06 mmol of lignin derivative (4-hydroxy-3-methoxybenzoic acid or 4-hydroxy-3,5-dimethoxybenzoic acid) or 0.1 g of lignin was placed into a 22.5 mL gas chromatography vial containing 5 mL of 0.1 mM NaNO<sub>2</sub> solution and the mixture was incubated for 24 h at room temperature. Afterwards, the products were extracted with 2 mL of methanol through solid phase extraction using a C18-bonded monolithic silica column (Bond Elut C18, 500 mg, 3 mL; VWR, Germany) and afterwards measured with a GC-MS (5973N, Agilent, Santa Clara, California, USA) (Kaiser and Benner, 2012).

## 2.5. Data analysis

N<sub>2</sub>O isotope ratios ( $R^{\alpha}$ ,  $R^{\beta}$  and  $R^{18\text{O}}$ ) were calculated based on the concentrations of <sup>14</sup>N<sup>14</sup>N<sup>16</sup>O, <sup>14</sup>N<sup>15</sup>N<sup>16</sup>O, <sup>15</sup>N<sup>14</sup>N<sup>16</sup>O, and <sup>14</sup>N<sup>14</sup>N<sup>18</sup>O obtained from QCLAS (section 2.1):

$$R^{\alpha} = \frac{{}^{14}\text{N}^{15}\text{N}^{16}\text{O}}{{}^{14}\text{N}^{14}\text{N}^{16}\text{O}} \quad (1)$$

$$R^{\beta} = \frac{{}^{15}\text{N}^{14}\text{N}^{16}\text{O}}{{}^{14}\text{N}^{14}\text{N}^{16}\text{O}} \quad (2)$$

$$R^{18O} = \frac{{}^{14}N^{14}N^{18}O}{{}^{14}N^{14}N^{16}O} \quad (3)$$

A drift correction was applied to all isotope ratios based on regular measurements of Cal1 at 36 ppm N<sub>2</sub>O. Thereafter, isotope ratios were converted to the  $\delta$ -notation in per mille by applying the following formula:

$$\delta_{A/B} = \left( \frac{R_A}{R_B} - 1 \right) \times 1000\text{‰} \quad (4)$$

2-point calculation was applied using Cal1 as the working standard according to Gröning (2018):

$$r\delta_{sam/std} = \delta_{sam/cal1} \times \frac{\delta_{cal2/std} - \delta_{cal1/std}}{\delta_{cal2/cal1}} + \delta_{cal1/std} \quad (5)$$

In Eq. (5), sam, std, cal1, and cal2 denote sample gas, international standard (air-N<sub>2</sub> for <sup>15</sup>N/<sup>14</sup>N, and VSMOW for <sup>18</sup>O/<sup>16</sup>O), and calibration gas 1 and 2, respectively,  $r\delta_{sam/std}$  is the raw  $\delta$  value of sample without a correction of N<sub>2</sub>O concentration dependency. Third-order polynomial regressions were applied to correct for the dependency of  $\delta^{15}N^\alpha$ ,  $\delta^{15}N^\beta$ , and  $\delta^{18}O$  on N<sub>2</sub>O concentration (Figure S1). Two regression equations were defined:  $f_{low}$  for the N<sub>2</sub>O range of 12–45 ppm, and  $f_{high}$  for the N<sub>2</sub>O range of 36–83 ppm. The R<sup>2</sup> values were higher than 0.99 for both  $f_{low}$  and  $f_{high}$ , and the differences of  $\delta$  values calculated by  $f_{low}$  and  $f_{high}$  at intermediate N<sub>2</sub>O concentrations from 36 to 45 ppm were lower than 0.5‰ (Figure S2), which indicates that both  $f_{low}$  and  $f_{high}$  were well fitted. The N<sub>2</sub>O concentration dependency was corrected according to the following equation:

$$\delta_{sam/std} = r\delta_{sam/std} + f(C_{cal1}) - f(C_{sam}) \quad (6)$$

In Eq. (6),  $r\delta_{sam/std}$  is the raw  $\delta$  value of the sample calculated based on Eq. (5),  $C_{cal1}$  is the average concentration of all the Cal1 measurements at around 36 ppm,  $C_{sam}$  denotes the N<sub>2</sub>O mixing ratio of the sample, and  $f$  denotes  $f_{low}$  when  $C_{sam}$  is equal to or lower than 36 ppm, but  $f_{high}$  when  $C_{sam}$  is higher than 36 ppm. Finally,  $\delta^{15}N^{bulk}$  was calculated as the average of  $\delta^{15}N^\alpha$  and  $\delta^{15}N^\beta$ :

$$\delta^{15}N^{bulk} \equiv (\delta^{15}N^\alpha + \delta^{15}N^\beta) / 2 \quad (7)$$

while SP<sub>N<sub>2</sub>O</sub> was determined using:

$$SP_{N_2O} \equiv \delta^{15}N^\alpha - \delta^{15}N^\beta \quad (8)$$

Net isotope effects  $\Delta^{15}\text{N}(\text{N}_2\text{O}/\text{NO}_2^-)$  and  $\Delta^{18}\text{O}(\text{N}_2\text{O}/\text{NO}_2^-)$  were calculated as the difference of  $\delta$  values of  $\text{N}_2\text{O}$  from that of  $\text{NO}_2^-$ , and then normalised based on the  $\text{N}_2\text{O}$  concentration:

$$\Delta^{15}\text{N}(\text{N}_2\text{O}/\text{NO}_2^-) = \sum((\delta^{15}\text{N}_{\text{N}_2\text{O}}^{\text{bulk}} - \delta^{15}\text{N}_{\text{NO}_2^-}) \times C_{\text{N}_2\text{O}}) / \sum C_{\text{N}_2\text{O}} \quad (9)$$

$$\Delta^{18}\text{O}(\text{N}_2\text{O}/\text{NO}_2^-) = \sum((\delta^{18}\text{O}_{\text{N}_2\text{O}} - \delta^{18}\text{O}_{\text{NO}_2^-}) \times C_{\text{N}_2\text{O}}) / \sum C_{\text{N}_2\text{O}} \quad (10)$$

The relative  $\text{N}_2\text{O}$  emission rate  $X_{\text{N}_2\text{O}}$  ( $\mu\text{mol N}_2\text{O mol}^{-1} \text{NO}_2^- \text{mol}^{-1} \text{s}^{-1}$  for lignin compounds and  $\mu\text{mol N}_2\text{O mol}^{-1} \text{NO}_2^- \text{kg}^{-1} \text{s}^{-1}$  for soil samples), was normalised for the reactants as follows:

$$X_{\text{N}_2\text{O}} = \frac{C_{\text{N}_2\text{O}} \times P \times F}{M_{\text{NO}_2^-} \times R \times T \times m} \quad (11)$$

$C_{\text{N}_2\text{O}}$  is the mixing ratio of  $\text{N}_2\text{O}$  (ppm) measured in real time at 1 Hz,  $P$  denotes the pressure in the reaction chamber (101325 Pa),  $F$  represents the flow rate of the carrier gas ( $\text{ml s}^{-1}$ ),  $R$  is the ideal gas constant ( $8.314 \text{ m}^3 \text{ Pa mol}^{-1} \text{ K}^{-1}$ ),  $T$  represents the temperature of the headspace in the reaction chamber (293.15 K),  $M_{\text{NO}_2^-}$  is the total applied  $\text{NO}_2^-$  (mol), and  $m$  is the amount of lignin compounds or soil (mol for lignin compounds and kg for soil). The manual dilution of  $\text{N}_2\text{O}$  mixing ratio with synthetic air was corrected with either a dilution factor or polynomial curve fitting. All of the calculations were conducted using MATLAB R2014b (MathWorks, Inc., USA).

### 3. RESULTS

#### 3.1. $\text{N}_2\text{O}$ isotopic composition from reactions of $\text{NO}_2^-$ with lignin derivatives

In the reaction of  $\text{NO}_2^-$  with organosolv lignin, approximately 8% of  $\text{NO}_2^-$  was converted to  $\text{N}_2\text{O}$  within 4 h, accounting for the highest relative  $\text{N}_2\text{O}$  emission rate (Fig. 2a). Compared with organosolv lignin, the reactions of  $\text{NO}_2^-$  with lignin-derived acids and aldehyde were much slower, with relative  $\text{N}_2\text{O}$  emission rates of less than  $900 \mu\text{mol N}_2\text{O mol}^{-1} \text{NO}_2^- \text{mol}^{-1} \text{s}^{-1}$ . The average relative  $\text{N}_2\text{O}$  emission rate decreased in the order: 4-hydroxy-3,5-dimethoxybenzoic acid > 4-hydroxybenzoic acid > 4-hydroxy-3-methoxybenzoic acid > 4-hydroxy-3,5-dimethoxybenzaldehyde (Table 3). In addition, the temporal trend of  $\text{N}_2\text{O}$  emission differed between lignin derivatives: the relative  $\text{N}_2\text{O}$  emission rate peaked within 1.2 h and decreased quickly afterwards in the treatment of 4-hydroxy-3,5-dimethoxybenzoic acid (Fig. 2m), while it took about 3 h to reach the maximum in the experiment

with 4-hydroxybenzoic acid (Fig. 2e). By contrast, the reaction rate changed gradually in the experiments with 4-hydroxy-3-methoxybenzoic acid and 4-hydroxy-3,5-dimethoxybenzaldehyde (Figs. 2i and 2q). pH increased by one unit in the first 4 h of the experiments with 4-hydroxybenzoic acid, 4-hydroxy-3-methoxybenzoic acid, and 4-hydroxy-3,5-dimethoxybenzoic acid, while it remained between approximately 2.7 and 6.1 in the experiments with organosolv lignin and 4-hydroxy-3,5-dimethoxybenzaldehyde, respectively.

A large variability of  $SP_{N_2O}$  values (from  $4.6 \pm 1.7\%$  to  $28.9 \pm 8.8\%$ ) was observed in reactions of  $NO_2^-$  with lignin and lignin-derived acids as well as aldehyde (Table 1). Most interestingly,  $SP_{N_2O}$  values of the same reaction also changed substantially over time. In the first 4 h,  $SP_{N_2O}$  values increased by approximately 5% in the treatment of 4-hydroxy-3,5-dimethoxybenzaldehyde (Fig. 2r), while they increased by more than 10% in the treatment of organosolv lignin (Fig. 2b). By contrast, no clear temporal trend was observed for the reaction of  $NO_2^-$  with 4-hydroxy-3-methoxybenzoic acid with  $SP_{N_2O}$  values ranging from 10 to 15% during the whole experiment (Fig. 2j). The  $SP_{N_2O}$  fluctuated largely by approximate 10% over time in the reaction of  $NO_2^-$  with 4-hydroxybenzoic acid and 4-hydroxy-3,5-dimethoxybenzoic acid (Figs. 2f and 2n).

The temporal trends of  $\delta^{18}O$  and  $\delta^{15}N^{bulk}$  of  $N_2O$  also differed in the reactions of  $NO_2^-$  with lignin and the four lignin-related compounds: both  $\delta^{18}O$  and  $\delta^{15}N^{bulk}$  of  $N_2O$  remained relatively stable in the experiments with 4-hydroxy-3,5-dimethoxybenzoic acid and 4-hydroxy-3,5-dimethoxybenzaldehyde, however, they varied by more than 12% in the reactions of  $NO_2^-$  with organosolv lignin and 4-hydroxybenzoic acid (Fig. 2). Correspondingly, the concentration-weighted net isotope effects  $\Delta^{15}N(N_2O/NO_2^-)$  and  $\Delta^{18}O(N_2O/NO_2^-)$  varied from -20.1 to -10.0‰ and from 10.2 to 19.5‰, respectively, in the reactions of  $NO_2^-$  with lignin derivatives (Table 3). No significant Rayleigh effects could be observed due to the low conversion ratio of  $NO_2^-$  to  $N_2O$ .

### 3.2. NO<sub>x</sub> emission and organic products from the reactions of NO<sub>2</sub><sup>-</sup> with lignin derivatives

Considerable NO<sub>x</sub> emission was observed in the reactions of NO<sub>2</sub><sup>-</sup> with lignin derivatives, and NO<sub>x</sub> emission increased to the maximum within 20 min, which was 1–2 h before N<sub>2</sub>O reached its maximum (Fig. 3). In the reaction of NO<sub>2</sub><sup>-</sup> with lignin, GC-MS analysis revealed the existence of various phenolic products including phenol, 3-methylphenol, 2-methoxyphenol, 4-ethylphenol, 2-methoxy-4-methylphenol, 4-ethyl-2-methoxyphenol, 2-methoxy-4-vinylphenol, 2,6-dimethoxyphenol, 2,6-dimethoxy-4-methylphenol, 2-methoxy-4-(1-propenyl)phenol, and 2,6-dimethoxy-4-[(1E)-prop-1-en-1-yl]phenol (Fig. 4a). While 2-methoxyphenol, 4-hydroxy-2-methoxybenzaldehyde, and 4-hydroxy-3-methoxybenzoic acid methyl ester were formed in the reaction of NO<sub>2</sub><sup>-</sup> with 4-hydroxy-3-methoxybenzoic acid (Fig. 4b), and 2,6-dimethoxyphenol and 4-hydroxy-3,5-dimethoxybenzohydrazide were formed in the reaction of NO<sub>2</sub><sup>-</sup> with 4-hydroxy-3,5-dimethoxybenzoic acid (Fig. 4c).

### 3.3. N<sub>2</sub>O isotopic signatures from NO<sub>2</sub><sup>-</sup> reactions in soils

N<sub>2</sub>O emissions from soil samples varied from approximately 0.73 to 5.64 μmol N<sub>2</sub>O mol<sup>-1</sup>NO<sub>2</sub><sup>-</sup> kg<sup>-1</sup> soil s<sup>-1</sup> in the order: forest soil > grassland soil > agriculture soil, and sterilisation did not inhibit the N<sub>2</sub>O emissions (Table 3). The concentration-weighted SP<sub>N<sub>2</sub>O</sub> values ranged from 17.9 ± 3.2‰ to 25.7 ± 2.3‰ in soils, which was within the SP<sub>N<sub>2</sub>O</sub> range of NO<sub>2</sub><sup>-</sup> reactions with lignin derivatives (Table 3). Similar to the treatments of lignin and its derivatives, temporal changes in SP<sub>N<sub>2</sub>O</sub> by more than 6‰ were observed in forest, grassland, and agricultural soils (Fig. 5). In contrast, the variability of δ<sup>18</sup>O and δ<sup>15</sup>N<sup>bulk</sup> between soil types was much smaller compared with SP<sub>N<sub>2</sub>O</sub> (Fig. 5). The real-time Δ<sup>15</sup>N(N<sub>2</sub>O/NO<sub>2</sub><sup>-</sup>) varied from -30 to -20‰ and from -27.7 to -21.9‰ in non-sterilised and sterilised soils, while Δ<sup>18</sup>O(N<sub>2</sub>O/NO<sub>2</sub><sup>-</sup>) changed from 14.4 to 22.5‰ and from 14.8 to 21.4‰ in non-sterilised and sterilised soils, respectively (Table 3).

## 4. DISCUSSIONS

### 4.1 N<sub>2</sub>O production pathways

Two different pathways, a hyponitrous acid pathway or a nitramide pathway (Fig. 6), have been discussed in relation to NO and N<sub>2</sub>O formation from the reaction of NO<sub>2</sub><sup>-</sup> with lignin derivatives (Austin, 1961; Kainz and Huber, 1959), which might therefore explain the different N<sub>2</sub>O production rates and shifting SP<sub>N<sub>2</sub>O</sub> values. Taking 4-hydroxybenzoic acid as an example, NO<sub>2</sub><sup>-</sup> is first protonated to HNO<sub>2</sub>, and the carboxyl group (-COOH) is subsequently substituted by a nitroso group (-NO) from HNO<sub>2</sub> to form CO<sub>2</sub> and 4-nitrosophenol (compound 1). The elimination of -COOH should account for the increase of pH in the treatments of 4-hydroxybenzoic acid, 4-hydroxy-3-methoxybenzoic acid, and 4-hydroxy-3,5-dimethoxybenzoic acid (Fig. 2). As 4-nitrosophenol is unstable at acidic pH, it partly decomposes to phenol (compound 4) and NO, while the other part is transformed to *p*-benzoquinone 4-oxime (compound 2) through rearrangement (Austin, 1961; Stevenson and Swaby, 1964). The formation of NO was confirmed in our experiments by high NO emission at the onset of the reactions measured with a chemiluminescence based analyser (Fig. 3). Similarly, 2-methoxyphenol and 2,6-dimethoxyphenol were detected as a product in the treatment of 4-hydroxy-3-methoxybenzoic acid (Fig. 4b) and 4-hydroxy-3,5-dimethoxybenzoic acid (Fig. 4c), respectively, which further confirmed the decarboxylation and the following removal of the nitroso group. Subsequently, the phenol can be attacked by another HNO<sub>2</sub> molecule through electrophilic substitution, resulting in the formation of 2-nitrosophenol (compound 5), which can rearrange to compound 6.

In the hyponitrous acid pathway, the C=N double bond of oximes can be subject to electrophilic attack of HNO<sub>2</sub> with a nitroso group being attached to the nitrogen atom and a hydroxyl group binding to the carbon atom, leading to the formation of hydroxyl-nitroso compounds (compounds 3 and 7) (Austin, 1961). Hydroxyl-nitroso compounds are very unstable and decompose quickly to hyponitrous acid (compound 8 and 9) and benzoquinones, with hyponitrous acid decomposing to N<sub>2</sub>O (Austin, 1961). In the nitramide pathway, electrophilic substitution, instead of electrophilic

addition, occurs at the nitrogen atom of the oximes with the production of nitramines (compounds 10 and 11), which decompose quickly to benzoquinones and nitramide (compound 12), and nitramide further decomposes to  $\text{N}_2\text{O}$  (Kainz and Huber, 1959). With the consumption of  $\text{NO}_2^-$  and 4-hydroxybenzoic acid, as well as the decomposition of nitroso compounds, pH slowly increased and the formation rate of  $\text{N}_2\text{O}$  decreased (Fig. 2).

The number and position of electrophilic functional groups attached to the aromatic ring can affect the reaction kinetics through mesomeric (+/-M) and inductive (+/-I) effects, as well as steric effects. On the one hand, a methoxy group ( $-\text{OCH}_3$ ) enhances the electron density of the aromatic ring by its +M effect, facilitating the electrophilic attack by  $\text{HNO}_2$  (or more precisely by the resulting nitrosonium ion  $\text{NO}^+$ ) especially in the ortho and para positions relative to the methoxy group, thereby accelerating the reaction. On the other hand,  $-\text{OCH}_3$  also hinders the formation of oximes to some extent through a steric effect, thus inhibiting  $\text{N}_2\text{O}$  production. In addition, acidic pH favours the protonation of  $\text{NO}_2^-$ , thereby promoting the reaction rate of  $\text{NO}_2^-$  with lignin compounds. Therefore, we hypothesise that the mesomeric and inductive effects can explain the much higher  $\text{N}_2\text{O}$  emission rate in the 4-hydroxy-3,5-dimethoxybenzoic acid treatment than in the 4-hydroxybenzoic acid treatment in the first hour of the reaction, while the higher pH could explain the lower  $\text{N}_2\text{O}$  production rate 2 h later (Figs. 2e and 2m). Even though the methoxy group in 4-hydroxy-3-methoxybenzoic acid increases the aromatic electron density, the increase in electron density is less pronounced as in 4-hydroxy-3,5-dimethoxybenzoic acid. This, in combination with the inhibitory steric effect of the methoxy group and the higher pH, could be the reason why the  $\text{N}_2\text{O}$  emission rate did not increase in the 4-hydroxy-3-methoxybenzoic acid treatment compared with 4-hydroxybenzoic acid in the first 3 h (Figs. 2e and 2i). In the case of 4-hydroxy-3,5-dimethoxybenzaldehyde, the aldehyde group first has to be oxidized to a carboxyl group before decarboxylation can occur on the one hand, and the pH higher than 6.0 limits the protonation of  $\text{NO}_2^-$  on the other hand. Therefore, the  $\text{N}_2\text{O}$  emission rate was much lower in the experiment with 4-hydroxy-3,5-dimethoxybenzaldehyde compared with 4-hydroxy-3,5-dimethoxybenzoic acid (Figs. 2m



and 2q). Since organosolv lignin is extracted with an organic solvent as one of the alternative chemical wood pulping techniques (Wei et al., 2017b), it has a higher content of reactive functional groups compared with other lignin derivatives (Fig. 4). The various reactive functional groups as well as the very low pH in the experiment with organosolv lignin helps to explain the drastically higher  $\text{N}_2\text{O}$  emission rate (Fig. 2a).

## 4.2. $\text{N}_2\text{O}$ isotopic signatures depending on reaction conditions

### 4.2.1 $SP_{\text{N}_2\text{O}}$

Real-time measurements of  $SP_{\text{N}_2\text{O}}$  from the reactions between  $\text{NO}_2^-$  and lignin derivatives over 4–6 hrs resulted in concentration-weighted average  $SP_{\text{N}_2\text{O}}$  values between  $13.4 \pm 3.8\text{‰}$  and  $24.4 \pm 1.0\text{‰}$  (Table 3). This is comparable to an earlier off-line study, where a large variability of  $SP_{\text{N}_2\text{O}}$  values (11.9–30‰) has been observed (Wei et al., 2017b). Remaining differences in  $SP_{\text{N}_2\text{O}}$  might be explained by a substantial longer incubation period in previous off-line experiments (24 h) (Wei et al., 2017b) in comparison to measurements conducted in the present study (4–6 h).  $SP_{\text{N}_2\text{O}}$  values for the reaction of  $\text{NO}_2^-$  with lignin derivatives observed in both studies (Wei et al., 2017b) also coincide with the ones collected from reactions of  $\text{NO}_2^-$  with SOM fractions at pH 3 (20–26‰) (Wei et al., 2017a), the chemical reduction of  $\text{NO}_2^-$  by ferrous iron at pH 7 under anaerobic conditions (10–22‰) (Jones et al., 2015), and the reaction of  $\text{NO}_2^-$  with trimethylamine borane at pH 1 (~30‰) (Toyoda et al., 2005). The significant progress in the present study, to the best of our knowledge, provides the first real-time dataset of  $SP_{\text{N}_2\text{O}}$  values for a number of exemplary reactions, which revealed a shift in  $SP_{\text{N}_2\text{O}}$  during the reactions. In the following, these temporal trends are discussed with respect to  $\text{N}_2\text{O}$  production pathways. Isotope effects of  $\text{N}_2\text{O}$  reduction are not considered, since it is very unlikely that  $\text{N}_2\text{O}$  is further reduced to  $\text{N}_2$  during chemodenitrification under oxic conditions.

According to the  $\text{N}_2\text{O}$  reaction mechanisms proposed above (Fig. 6), hyponitrous acid and nitramide are supposed to be the direct precursors of  $\text{N}_2\text{O}$  formation from the reaction of  $\text{NO}_2^-$  with lignin derivatives. For the symmetric hyponitrous acid molecule, isotope effects during its

decomposition are probably the key factor controlling  $SP_{N_2O}$  values. Theoretical calculations using density functional theory (DFT) calculations by Fehling and Friedrichs (2011) predict the formation of both *cis*- and *trans*-hyponitrous acid, and substantially different  $SP_{N_2O}$  values for  $N_2O$  formation via both intermediates. While a low  $SP_{N_2O}$  value is predicted for the reaction via *trans*-hyponitrous acid (-15‰), a much higher value is assumed for *cis*-hyponitrous acid decomposition (31‰) (Fehling, 2012). In principle, the formation of *trans*-hyponitrous acid from hydroxyl-nitroso compounds is favoured due to steric effects, however, *trans*-hyponitrous acid could be isomerised to *cis*-hyponitrous acid through a fast acid-base equilibrium which generally dominates under strongly acidic conditions (Bringas et al., 2016; Fehling and Friedrichs, 2011). Hyponitrous acid is also proposed as the key precursor in microbial  $N_2O$  production. During the oxidation of  $NH_2OH$  to  $N_2O$  by HAO, a  $NH_2OH$  molecule is first bound to the enzyme, then a second  $NH_2OH$  molecule attacks the N atom of the first, leading to the formation of a *cis*-hyponitrous acid-like N-N bond (Yamazaki et al., 2014). Finally,  $N_2O$  with a  $SP_{N_2O}$  value of 30–36‰ is generated through the cleavage of the OH group of the first  $NH_2OH$  molecule (Yamazaki et al., 2014). The NO reduction by fungal NO reductase (NOR) to  $N_2O$  follows a mechanism that is similar with the  $NH_2OH$  oxidation by HAO, as two NO molecules are sequentially bound to NOR and form a *cis*-hyponitrite-like compound which decomposes quickly to  $N_2O$  with a  $SP_{N_2O}$  of 35–37‰ (Obayashi et al., 1998; Rohe et al., 2014; Sutka et al., 2008). By contrast, during bacterial denitrification, two NO molecules are simultaneously bound to the enzyme and a *trans*-hyponitrite-like compound is formed (Watmough et al., 2009), which further decomposes to  $N_2O$  with a  $SP_{N_2O}$  of around zero.

In the nitramide pathway, the N atoms of the first- and second-bound nitroso group act as the terminal ( $N^\beta$ ) and central ( $N^\alpha$ ) nitrogen atoms of the  $N_2O$  molecule, respectively. Nitramide formation is the rate-determining step, hence kinetic isotope effects during nitramide formation are supposed to dominate the  $N_2O$  isotopic composition. Since the cleavage of the N=C bond favours  $^{15}N^\beta$  depletion but the formation of the N-N bond of nitramines favours  $^{15}N^\alpha$  enrichment, we speculate that the  $SP_{N_2O}$  value via the nitramide pathway should be significantly higher than zero. Consequently, both

the nitramide and *cis*-hyponitrous acid pathways favour higher  $SP_{N_2O}$ , while the *trans*-hyponitrous acid pathway favors lower  $SP_{N_2O}$ . The temporal changes of  $SP_{N_2O}$  values could result from the varying ratio of  $N_2O$  being produced via the *trans*-hyponitrous acid with respect to the sum of  $N_2O$  produced via nitramide and *cis*-hyponitrous acid.

The electrophilic attack and the formation of hyponitrous acid can be facilitated by acidic pH. By contrast, the formation of nitramide is favoured at higher pH. Therefore, the increase in pH could account for the dramatic drop of  $N_2O$  production rate, accompanied by an increase of  $SP_{N_2O}$ , at the end of the experiment with 4-hydroxybenzoic acid and 4-hydroxy-3,5-dimethoxybenzoic acid (Fig. 2).

#### 4.2.2 Net isotope effects

The net  $^{15}N$  isotope effect,  $\Delta^{15}N$  ( $N_2O/NO_2^-$ ), observed in this study is within the range of values reported in previous studies on chemodenitrification (Grabb et al., 2017; Jones et al., 2015; Wei et al., 2017b), but slightly higher than that of nitrifier denitrification (Sutka et al., 2006). Isotope effects are affected by the reaction kinetics and they are generally determined by the rate-limiting step (Snider et al., 2009), such as the formation of hyponitrous acid and nitramide in the reactions of lignin derivatives with  $NO_2^-$ . The cleavage of  $^{14}N-C$  to form hyponitrous acid and  $^{14}N=C$  to form nitramide are preferred over the cleavage of  $^{15}N-C$  and  $^{15}N=C$  bonds. Therefore  $^{15}N$  depletion was observed in the chemical reduction of  $NO_2^-$  to  $N_2O$  by lignin derivatives (Table 3). Even though  $N_2O$  reduction leads to an increase of  $\delta^{15}N^{bulk}$  of the remaining  $N_2O$  pool by 2-7‰ (Ostrom et al., 2007), this process is not relevant during chemodenitrification, hence the variation of  $\Delta^{15}N$  ( $N_2O/NO_2^-$ ) during the reactions of this study (Fig. 2) are likely resulting from the dynamic change of hyponitrous acid and nitramide formation rates, dependent on substrate availability and pH.

The concentration-weighted net  $^{18}O$  isotope effect,  $\Delta^{18}O$  ( $N_2O/NO_2^-$ ), ranged from 10.2 to 20.2‰ (Table 3), which is in a similar range of previously reported values (Grabb et al., 2017; Jones et al., 2015; Wei et al., 2017b). The value of  $\Delta^{18}O$  ( $N_2O/NO_2^-$ ) found in the present study is much higher than that of nitrifier denitrification (Sutka et al., 2006), but much lower than that of fungal

denitrification (Rohe et al., 2014; Sutka et al., 2008). Apart from the kinetic isotope effect of  $\text{N}_2\text{O}$  production,  $\Delta^{18}\text{O}$  ( $\text{N}_2\text{O}/\text{NO}_2^-$ ) is also strongly influenced by O exchange with water. Depending on different  $\text{N}_2\text{O}$  production mechanisms, O exchange of substrates with water can vary from approximately 2% to more than 90% (Kool et al., 2007). In the reactions of lignin derivatives with  $\text{NO}_2^-$ , O exchange could occur both between nitrite itself and water and between the hydroxyl groups of hyponitrous acid and nitramide. However, the rate and degree of O exchange during formation of hyponitrous acid and nitramide are currently unclear and should be explored in future studies.

### 4.3 Chemodenitrification and $\text{N}_2\text{O}$ source partitioning

#### 4.3.1 Chemodenitrification in soil

Recently, increasing evidence is provided for the central role of  $\text{NO}_2^-$  in the soil N cycle and particularly in  $\text{N}_2\text{O}$  emission (Maharjan and Venterea, 2013; Venterea, 2007). In the present study, we also found that  $\text{NO}_2^-$  led to  $\text{N}_2\text{O}$  emission in all of the three types of soils (Fig. 3), equivalent to  $43.2\text{--}483.8 \mu\text{mol N}_2\text{O mol}^{-1} \text{NO}_2^- \text{kg}^{-1} \text{soil d}^{-1}$ , which is in a similar range as in previous studies where chemodenitrification dominated (Ostrom et al., 2016; Venterea, 2007; Wei et al., 2017a). As  $\text{NO}_2^-$  - related  $\text{N}_2\text{O}$  production in unsterilised soils may include microbial pathways, e.g. denitrification and nitrifier denitrification, and chemodenitrification (Wankel et al., 2017), sterilised soil samples were also analysed in the present study. Instead of decreasing  $\text{N}_2\text{O}$  production, autoclaving increased the  $\text{N}_2\text{O}$  emission rate dramatically, which could be explained by an increased solubility of SOM after autoclaving, accelerating the reactivity of the soil to  $\text{NO}_2^-$  (Berns et al., 2008). In addition, the values of  $\text{SP}_{\text{N}_2\text{O}}$ ,  $\delta^{18}\text{O}$ , and  $\delta^{15}\text{N}^{\text{bulk}}$  were within the range of  $\text{NO}_2^-$ -lignin reactions in chemical assays and they changed in a similar trend in sterilised and unsterilised soil samples (Fig. 3), indicating that chemodenitrification was the main  $\text{N}_2\text{O}$  source in soils after  $\text{NO}_2^-$  application and accounted for the shifts of  $\text{N}_2\text{O}$  isotopic composition.

#### 4.3.2 N<sub>2</sub>O source partitioning

Even though  $SP_{N_2O}$  is widely used for N<sub>2</sub>O source partitioning, it still remains an open question of whether it is sufficiently conclusive or not (Decock and Six, 2013; Wei et al., 2017b). The reliability of using isotopic signatures in N<sub>2</sub>O source partitioning highly depends on the robustness of N<sub>2</sub>O isotopic signatures of certain N<sub>2</sub>O production and reduction processes. The ranges of  $SP_{N_2O}$ ,  $\delta^{15}N^{bulk}$ , and  $\delta^{18}O$  have been observed to be 6.0 to 37.4‰, -41.0 to -3.9‰, and 14 to 44.6‰ for chemodenitrification (Jones et al., 2015; Toyoda et al., 2005; Wei et al., 2017b), -11 to 1.4‰, -34.8 to -8.8‰, and 10 to 20‰ for bacterial denitrification (Toyoda et al., 2005; Zou et al., 2014), 34 to 40‰, -34 to -21.9‰, and 30 to 40‰ for fungal denitrification (Sutka et al., 2008), and 27 to 37‰, -61.4 to -40.3‰, and 40 to 50‰ for nitrification (Sutka et al., 2006), respectively (Fig. 7a). Net isotope effects of  $\Delta^{15}N(N_2O/NO_2^-)$  and  $\Delta^{18}O(N_2O/NO_2^-)$ , have been observed in ranges of -28.1 to 9.6‰ and 3 to 24.2‰ for chemodenitrification (Grabb et al., 2017; Jones et al., 2015; Wei et al., 2017b), -39.5 to -31.4‰ and 7.0 to 9.8‰ for nitrifier denitrification (Sutka et al., 2006), and -29.0 to -8.8‰ and 55.8 to 60.8‰ for fungal denitrification (Rohe et al., 2014; Sutka et al., 2008), respectively (Fig. 7b).

Due to the distinct  $^{15}N$  and  $^{18}O$  isotopic effects,  $\Delta^{15}N(N_2O/NO_2^-)$  and  $\Delta^{18}O(N_2O/NO_2^-)$  of chemodenitrification are clearly separated from the corresponding values of fungal denitrification and nitrifier denitrification (Fig. 7b). Even though  $\delta^{15}N^{bulk}$  and  $\delta^{18}O$  of N<sub>2</sub>O of chemodenitrification are also clearly distinct from bacterial denitrification, they strongly overlap with fungal denitrification and nitrification in the end-member map (Fig. 7a). To date, only few data of  $\Delta^{15}N(N_2O/NO_2^-)$  and  $\Delta^{18}O(N_2O/NO_2^-)$  from  $NO_2^-$ -related N<sub>2</sub>O production have been published (Rohe et al., 2014; Sutka et al., 2006; Sutka et al., 2008), and further studies are needed to explore the isotope effects of N<sub>2</sub>O production under various conditions.

Since the range of  $SP_{N_2O}$  values of chemodenitrification is in the intermediate zone between fungal denitrification and nitrifier denitrification, a classical two-end-member mixing model (Zhang et al., 2016) fails to quantify N<sub>2</sub>O sources unambiguously. Therefore, a more sophisticated model involving both  $SP_{N_2O}$  and isotope effects is needed for more reliable N<sub>2</sub>O source partitioning. Similarly,

SP<sub>N<sub>2</sub>O</sub> values encompassed the ranges of microbial nitrification (33 to 37‰) and denitrification (-10 to 0‰) in the McMurdo Dry Valleys, Antarctica, even though chemodenitrification accounted for most of the N<sub>2</sub>O emission (Peters et al., 2014). Further, the application of SP<sub>N<sub>2</sub>O</sub> also failed to attribute source processes of N<sub>2</sub>O in Lake Vida, Victoria Valley, Antarctica (Ostrom et al., 2016; Zhu-Barker et al., 2015) and in the Don Juan Pond, Antarctica (Samarkin et al., 2010), where chemodenitrification with distinguishable N<sub>2</sub>O isotope signatures acted as the main N<sub>2</sub>O source.

## 5. CONCLUSION

Biotic ammonium oxidation and nitrate reduction provide NO<sub>2</sub><sup>-</sup> sources for chemodenitrification. On the other hand, chemodenitrification and biotic N<sub>2</sub>O production processes, including nitrification and denitrification, compete for NO<sub>2</sub><sup>-</sup>. In agreement with a previous study (Wei et al., 2017b), we found that SP<sub>N<sub>2</sub>O</sub> values of chemodenitrification varied largely in experiments with different lignin derivatives, and end-member maps of N<sub>2</sub>O isotopic signatures become highly limited for N<sub>2</sub>O source partitioning when chemodenitrification is taken into account. Furthermore, this laboratory study demonstrated that the N<sub>2</sub>O isotopic signatures of chemodenitrification also changed over time during the reaction, which contributes to the temporary variation of N<sub>2</sub>O isotopic composition in soils. Two different N<sub>2</sub>O production mechanisms with hyponitrous acid or nitramide as intermediate would very likely explain the temporal changes of SP<sub>N<sub>2</sub>O</sub> during the reactions studied, which deserve to be further explored. Due to the large variability and uncertainty of N<sub>2</sub>O isotopic signatures from chemodenitrification, additional constraints, such as a combination of N<sub>2</sub>O isotopic composition with N and O isotope effects, novel clumped-isotopes or triple oxygen isotopic information, are needed for making N<sub>2</sub>O source partitioning unambiguous.

**Table 1.** Characteristics of the soil samples. The indicated precision is the standard deviation for replicate sample measurements (n = 3).

Soil sample	Soil pH	Total N (mg g <sup>-1</sup> )	Total C (%)	C/N	WHC <sup>a</sup> (%)	Fe (mg g <sup>-1</sup> )	Mn (mg g <sup>-1</sup> )
Forest soil	3.5 ± 0.0	14.6 ± 0.0	30.1 ± 0.8	20.6 ± 0.6	137.0 ± 0.1	29.0 ± 3.0	2.20 ± 0.12
Grassland soil	5.1 ± 0.0	12.8 ± 0.1	4.62 ± 0.02	3.6 ± 0.1	80.0 ± 1.2	33.5 ± 1.5	1.40 ± 0.40
Agricultural soil	6.0 ± 0.2	1.4 ± 0.1	1.28 ± 0.01	9.1 ± 0.2	35.0 ± 4.2	11.7 ± 0.2	0.46 ± 0.03

Note:

<sup>a</sup> WHC, water holding capacity.

**Table 2.** Experimental details for individual treatment.

Lignin derivative/soil sample	Lignin derivative (mmol)/soil (g)	Nitrite (mmol)	Water (mL)	Flow rate (mL min <sup>-1</sup> )
organosolv lignin <sup>a</sup>	3.3	0.1 – 0.2	50	16 – 32
4-hydroxybenzoic acid	57.9	20.0	50	16
4-hydroxy-3-methoxybenzoic acid	59.5	23.5	50	16 – 32
4-hydroxy-3,5-dimethoxybenzoic acid	40.4	27.9	50	16 – 32
4-hydroxy-3,5-dimethoxybenzaldehyde	34.0	58.8	50	16
non-sterilised forest soil	10.0	18.8 – 31.8	50	16 – 32
non-sterilised grassland soil	10.0	17.6 – 29.4	50	16
non-sterilised agricultural soil	10.0	17.6 – 29.4	50	16
sterilised forest soil	10.0	29.4 – 35.3	50	12.8 – 16
sterilised grassland soil	10.0	6.5 – 9.2	50	16 – 20
sterilised agricultural soil	10.0	11.8 – 13.5	50	16 – 18.4

Note:

<sup>a</sup> organosolv lignin is estimated as C<sub>81</sub>H<sub>92</sub>O<sub>28</sub> with molecular weight of 1513.6 g mol<sup>-1</sup> according to PubChem.

**Table 3** Net isotope effect of  $^{15}\text{N}$  and  $^{18}\text{O}$ ,  $\text{N}_2\text{O}$  site preference ( $\text{SP}_{\text{N}_2\text{O}}$ ), and  $\text{N}_2\text{O}$  production rate of the reaction of nitrite with different organic compounds and soil samples. Results are shown as the average values  $\pm$  standard deviation of three replicates.

	$\Delta^{15}\text{N}(\text{N}_2\text{O}/\text{NO}_2^-)$ (‰ vs. air- $\text{N}_2$ )			$\Delta^{18}\text{O}(\text{N}_2\text{O}/\text{NO}_2^-)$ (‰ vs. VSMOW)			$\text{SP}_{\text{N}_2\text{O}}$ (‰)			Relative $\text{N}_2\text{O}$ production rate <sup>c</sup>		
	Max. <sup>a</sup>	Min. <sup>a</sup>	Avg. <sup>b</sup>	Max.	Min.	Avg.	Max.	Min.	Avg.	Max.	Min.	Avg.
Organosolv lignin	-3.1 $\pm$ 4.8	-17.8 $\pm$ 4.0	-10.0 $\pm$ 4.1	21.4 $\pm$ 1.2	16.0 $\pm$ 0.9	19.5 $\pm$ 1.7	28.8 $\pm$ 0.2	12.1 $\pm$ 1.7	24.4 $\pm$ 1.0	940 $\pm$ 37	475 $\pm$ 156	810 $\pm$ 33
4-hydroxybenzoic acid	-7.1 $\pm$ 4.5	-22.8 $\pm$ 0.8	-15.4 $\pm$ 1.2	17.0 $\pm$ 2.2	4.7 $\pm$ 3.7	10.2 $\pm$ 3.4	25.6 $\pm$ 1.4	7.7 $\pm$ 2.8	19.5 $\pm$ 0.5	0.28 $\pm$ 0.0	0.10 $\pm$ 0.02	0.19 $\pm$ 0.02
4-hydroxy-3-methoxybenzoic acid	-14.8 $\pm$ 3.9	-20.9 $\pm$ 4.2	-17.7 $\pm$ 3.9	19.4 $\pm$ 4.7	10.3 $\pm$ 0.9	13.3 $\pm$ 1.6	20.5 $\pm$ 6.4	7.3 $\pm$ 5.4	13.4 $\pm$ 3.8	0.20 $\pm$ 0.02	0.08 $\pm$ 0.02	0.15 $\pm$ 0.01
4-hydroxy-3,5-dimethoxybenzoic acid	-9.9 $\pm$ 0.3	-18.3 $\pm$ 0.4	-13.0 $\pm$ 0.5	20.2 $\pm$ 2.9	7.2 $\pm$ 2.1	12.2 $\pm$ 0.4	28.9 $\pm$ 8.8	4.6 $\pm$ 1.7	15.4 $\pm$ 1.7	0.90 $\pm$ 0.11	0.00 $\pm$ 0.13	0.33 $\pm$ 0.02
4-hydroxy-3,5-dimethoxybenzaldehyde	-17.7 $\pm$ 3.8	-22.6 $\pm$ 1.9	-20.1 $\pm$ 2.8	20.6 $\pm$ 3.2	16.5 $\pm$ 2.7	18.9 $\pm$ 2.8	23.2 $\pm$ 3.4	13.7 $\pm$ 4.0	19.2 $\pm$ 2.6	0.12 $\pm$ 0.02	0.09 $\pm$ 0.02	0.11 $\pm$ 0.02
non-sterilised agricultural soil	-20.0 $\pm$ 5.2	-26.6 $\pm$ 2.4	-22.7 $\pm$ 4.8	22.5 $\pm$ 2.7	17.3 $\pm$ 3.3	20.2 $\pm$ 2.4	31.1 $\pm$ 3.3	14.8 $\pm$ 0.9	22.1 $\pm$ 0.6	0.84 $\pm$ 0.12	0.42 $\pm$ 0.12	0.55 $\pm$ 0.02
sterilised agricultural soil	-24.0 $\pm$ 2.8	-27.7 $\pm$ 2.2	-25.8 $\pm$ 2.6	21.2 $\pm$ 2.3	17.6 $\pm$ 0.7	19.4 $\pm$ 1.3	29.2 $\pm$ 4.1	21.3 $\pm$ 0.8	25.7 $\pm$ 2.3	1.81 $\pm$ 1.21	1.03 $\pm$ 0.13	1.22 $\pm$ 0.27
non-sterilised forest soil	-20.8 $\pm$ 5.8	-24.0 $\pm$ 5.5	-22.8 $\pm$ 5.8	20.6 $\pm$ 0.9	16.4 $\pm$ 1.3	17.8 $\pm$ 1.6	21.2 $\pm$ 1.3	15.9 $\pm$ 0.8	18.6 $\pm$ 1.1	2.51 $\pm$ 0.07	1.21 $\pm$ 0.48	2.23 $\pm$ 0.08
sterilised forest soil	-22.3 $\pm$ 0.8	-26.6 $\pm$ 0.7	-23.9 $\pm$ 0.8	20.3 $\pm$ 0.9	14.8 $\pm$ 2.4	16.8 $\pm$ 1.7	25.9 $\pm$ 1.5	17.4 $\pm$ 1.4	20.1 $\pm$ 0.9	6.06 $\pm$ 0.35	3.70 $\pm$ 0.38	5.64 $\pm$ 0.38
non-sterilised grassland soil	-21.6 $\pm$ 4.3	-30.0 $\pm$ 2.8	-25.2 $\pm$ 3.1	20.9 $\pm$ 4.0	14.4 $\pm$ 3.4	17.9 $\pm$ 3.3	24.8 $\pm$ 2.2	12.2 $\pm$ 5.1	17.9 $\pm$ 3.2	0.92 $\pm$ 0.13	0.56 $\pm$ 0.20	0.73 $\pm$ 0.20
sterilised grassland soil	-21.9 $\pm$ 1.6	-25.9 $\pm$ 2.6	-23.9 $\pm$ 2.1	21.4 $\pm$ 1.3	17.4 $\pm$ 1.1	19.5 $\pm$ 1.2	29.1 $\pm$ 1.0	19.2 $\pm$ 3.9	23.2 $\pm$ 2.7	2.75 $\pm$ 0.60	1.99 $\pm$ 0.16	2.18 $\pm$ 0.18

Note:

<sup>a</sup> Max. and Min. values are the real-time maximum and minimum values, respectively.

<sup>b</sup> Avg. values were concentration-weighted over the complete experimental run.

<sup>c</sup> The unit of relative  $\text{N}_2\text{O}$  production rate is  $\mu\text{mol N}_2\text{O mol}^{-1} \text{NO}_2^- \text{mol}^{-1}$  compound  $\text{s}^{-1}$  for lignin and lignin derivatives, and  $\mu\text{mol N}_2\text{O mol}^{-1} \text{NO}_2^- \text{kg}^{-1}$  soil  $\text{s}^{-1}$  for soil samples



# Figures

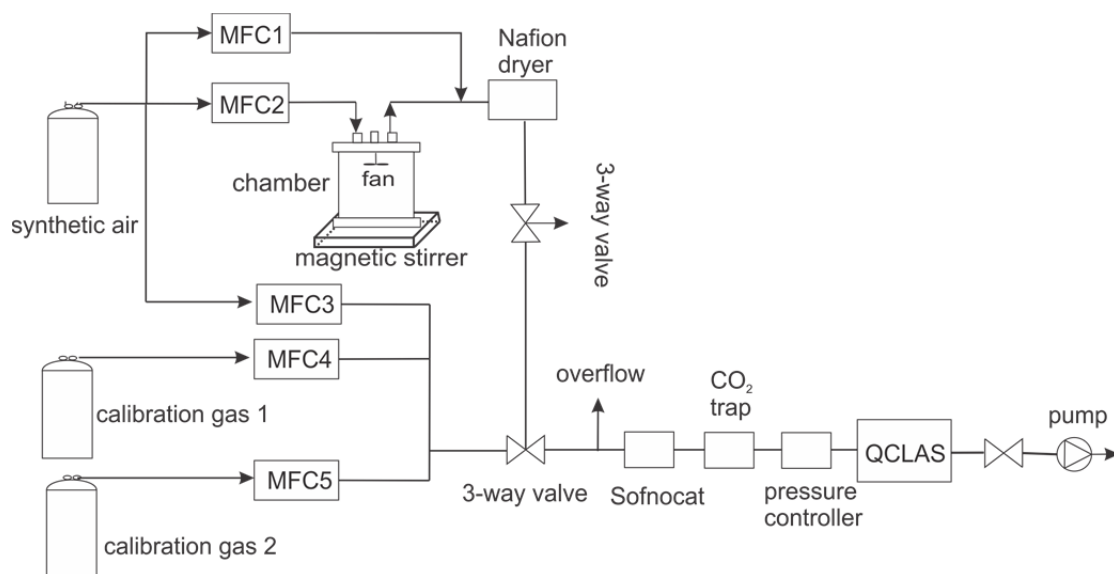
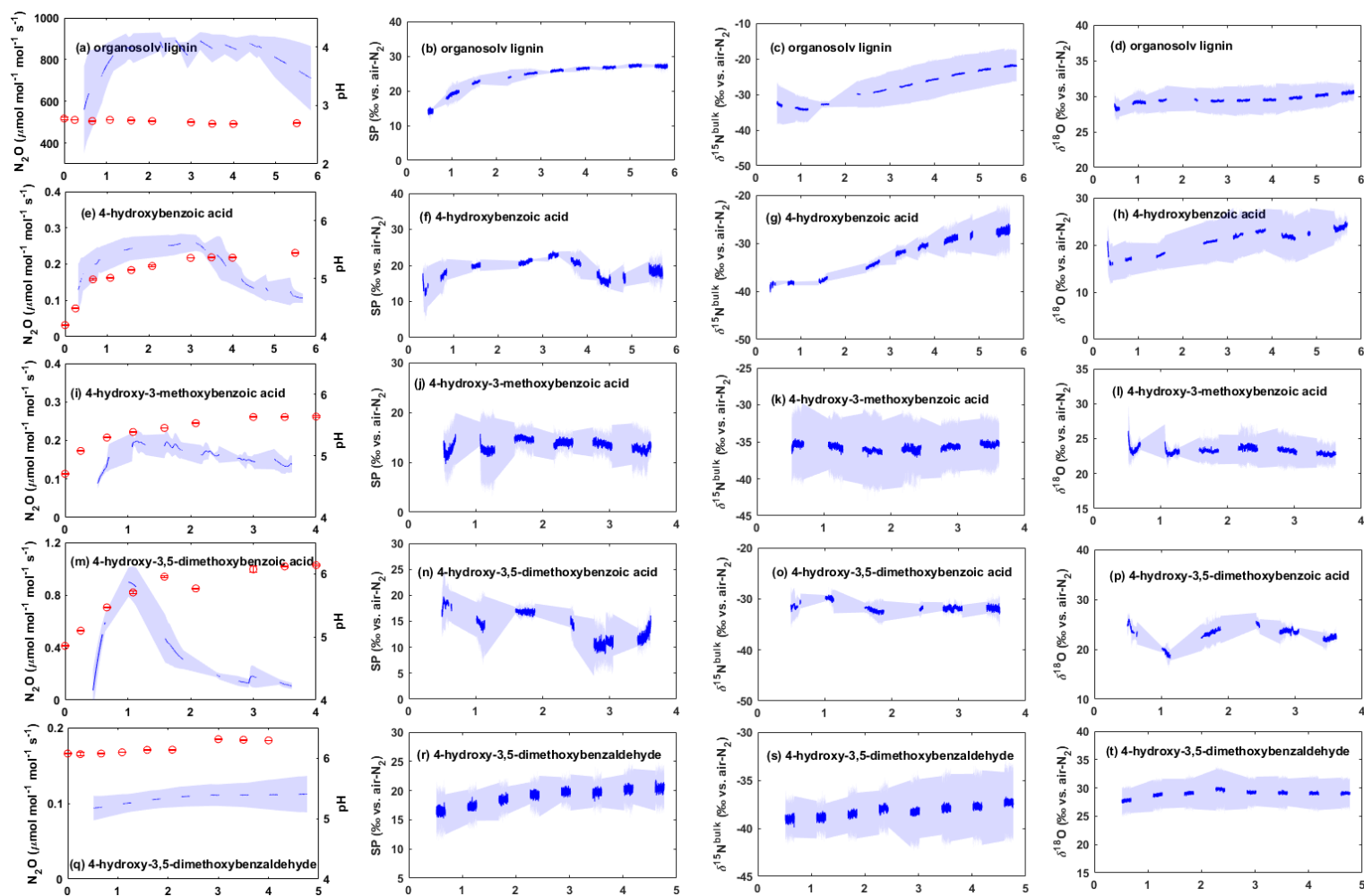


**Fig. 1.** Schematic diagram of the setup used for real-time measurement of N<sub>2</sub>O isotopic signatures.

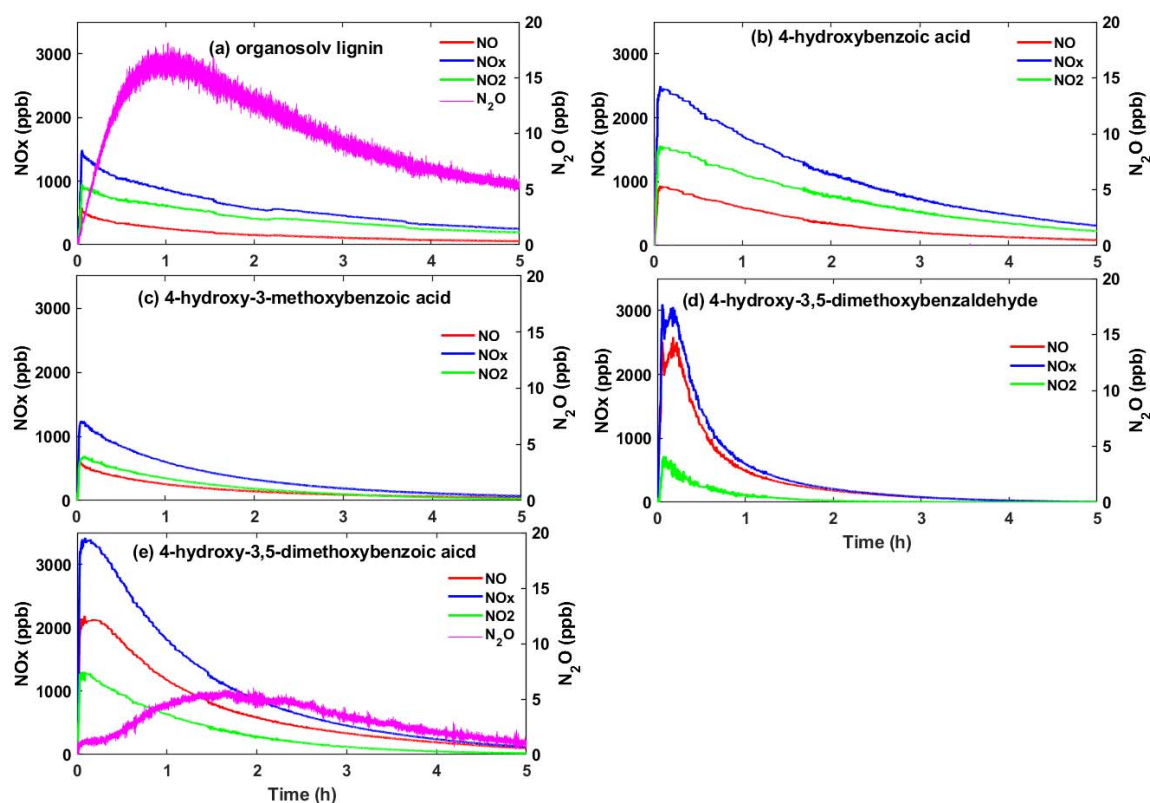


558

559 **Fig. 2.** Reaction of  $\text{NO}_2^-$  with organosolv lignin and lignin derivatives. Blue dots are the mean  $\text{N}_2\text{O}$  production rates and isotopic signatures of triplicates, the  
 560 shaded areas indicate the standard deviation (SD), periods without sample measurement are linearly interpolated. Red dots represent mean pH  $\pm$  SD of  
 561 triplicates.

562

563



564

565 **Fig. 3.** Simultaneous  $N_2O$  and  $NO_x$  ( $NO + NO_2$ ) emissions from the reactions of nitrite with organosolv  
 566 lignin (a), 4-hydroxybenzoic acid (b), 4-hydroxy-3-methoxybenzoic acid (c), 4-hydroxy-3,5-  
 567 dimethoxybenzaldehyde (d), 4-hydroxy-3,5-dimethoxybenzoic acid (e). The  $N_2O$  mixing ratio in the  
 568 treatments of 4-hydroxybenzoic acid, 4-hydroxy-3-methoxybenzoic acid, and 4-hydroxy-3,5-  
 569 dimethoxybenzaldehyde was lower than the detection limit.

570

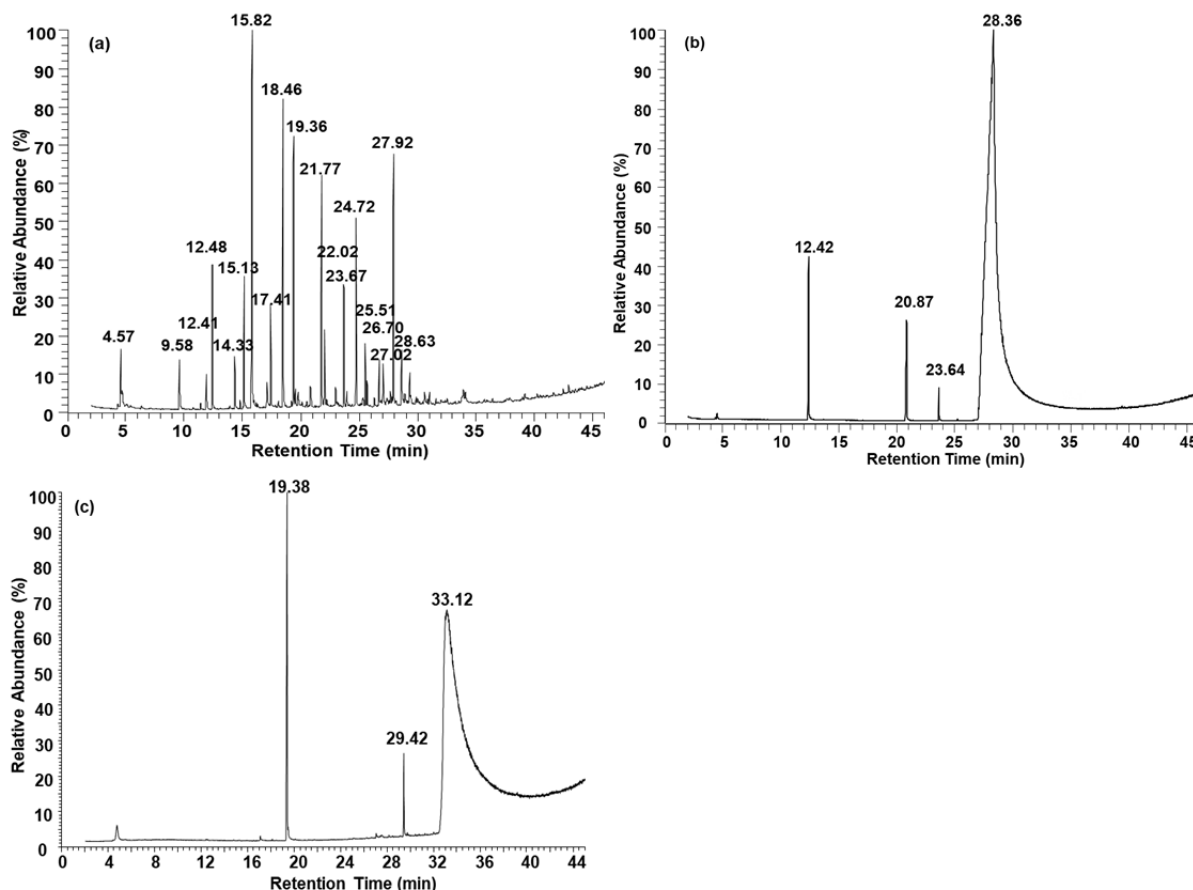
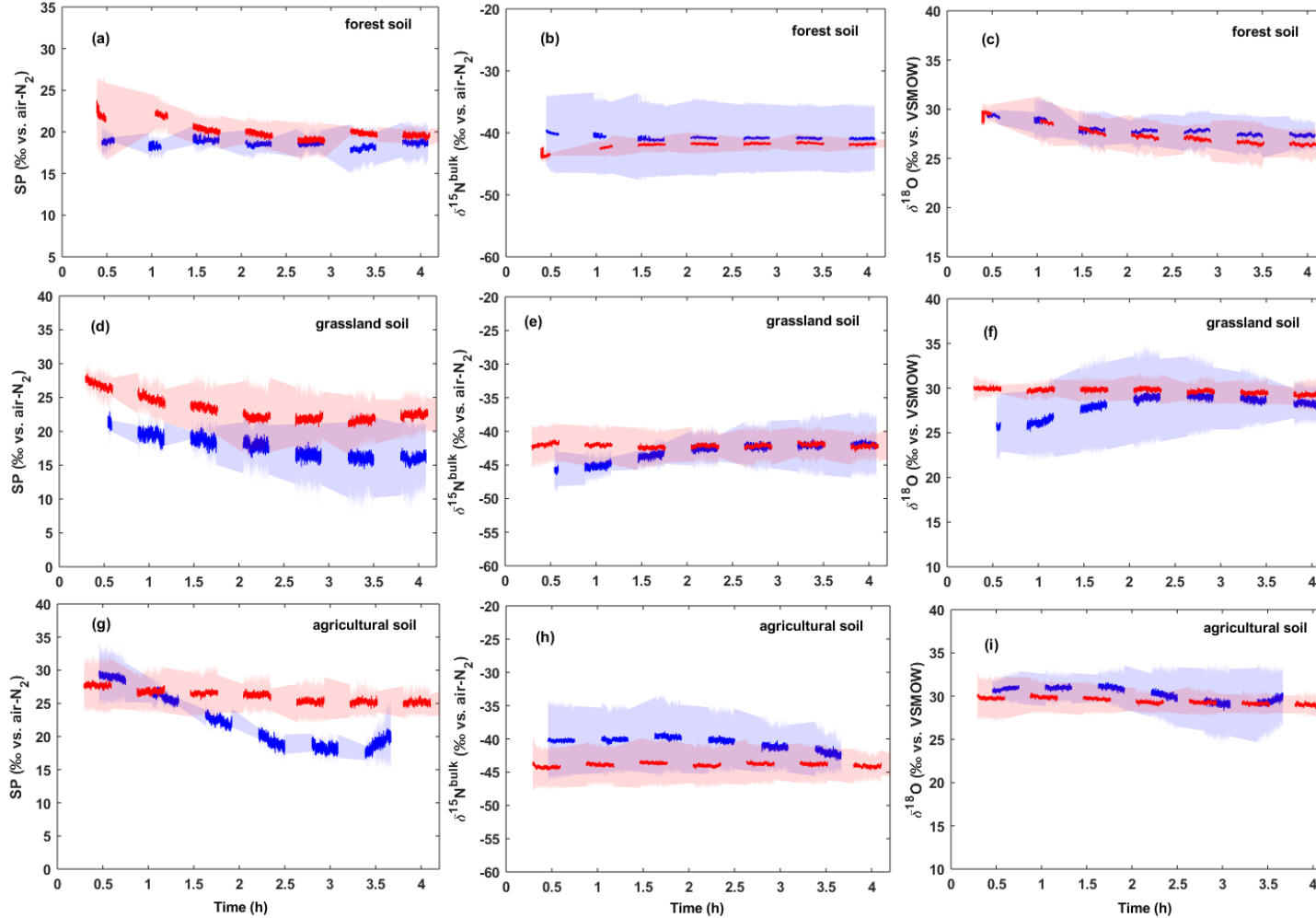


**Fig. 4.** Gas chromatography–mass spectrometry spectrum of products from the reaction of nitrite with organosolv lignin (a), 4-hydroxy-3-methoxybenzoic acid (b), and 4-hydroxy-3,5-dimethoxybenzoic acid (c). Compounds in (a) represent (2-aziridinyloxy)phenol, 3-methylphenol, 2-methoxyphenol, 4-ethylphenol, 2-methoxy-4-methylphenol, 4-methylbenzaldehyde, 4-ethyl-2-methoxyphenol, 2-methoxy-4-vinylphenol, 2,6-dimethoxyphenol, 2,6-dimethoxy-4-methylphenol, 2-methoxy-4-(1-propenyl)phenol, 1,2,3-trimethoxy-5-methylbenzene, 2-(3,4-dimethoxyphenyl)-6-methyl-3,4-chromanediol, 2,6-dimethoxy-4-(1E)-1-propen-1-yl-phenol, 2,6-dimethoxy-4-(1E)-1-propen-1-yl-phenol, 4-hydroxy-3,5-dimethoxybenzaldehyde, 2,6-dimethoxy-4-(1E)-1-propen-1-yl-phenol, 1-(4-hydroxy-3,5-dimethoxyphenyl)ethanone at retention time ( $t_R$ ) of 4.57, 9.58, 12.41, 12.48, 14.33, 15.13, 15.82, 17.41, 18.46, 19.36, 21.77, 22.02, 23.67, 24.72, 25.51, 26.70, 27.02, 27.92, 28.63 min, respectively. Compounds in (b) stand for 2-methoxyphenol, 4-hydroxy-2-methoxybenzaldehyde, 4-hydroxy-3-methoxybenzoic acid methyl ester, 4-hydroxy-3-methoxybenzoic acid at  $t_R$  of 12.42, 20.87, 23.64, 28.36 min, respectively. Compounds in (c) are 2,6-dimethoxyphenol at  $t_R$  of 19.38 min, 4-hydroxy-3,5-dimethoxybenzohydrazide at  $t_R$  of 29.42 min, and 4-hydroxy-3,5-dimethoxybenzoic acid at  $t_R$  of 33.12 min.

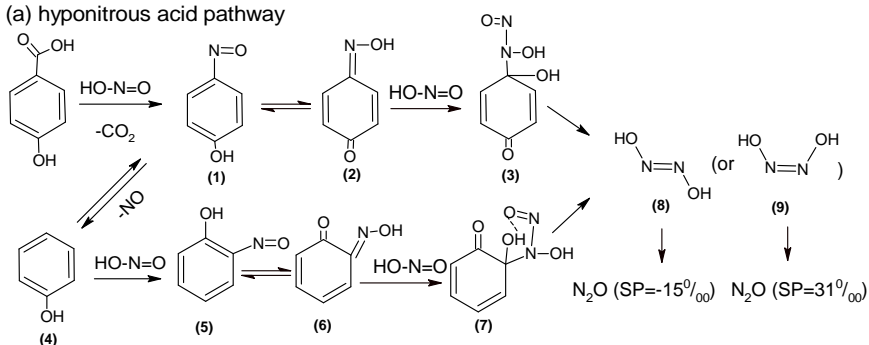


588

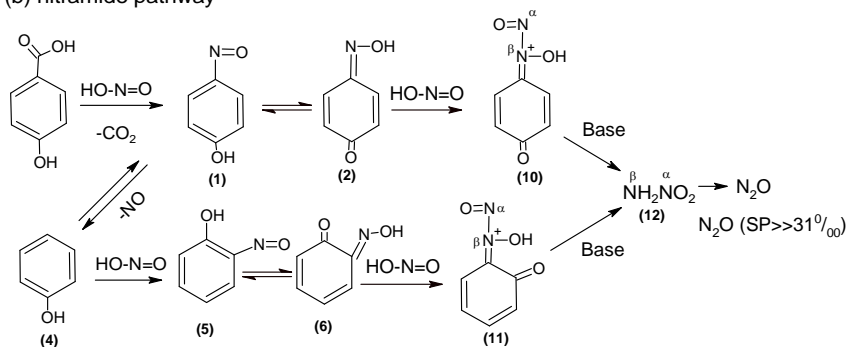
589 **Fig. 5.** Isotopic signatures of  $\text{NO}_2^-$  related  $\text{N}_2\text{O}$  emission in forest, agricultural, and grassland soils. Shown are mean values of three replicates in unsterilized  
 590 (blue dots) and sterilized (red dots) soils. The shaded areas indicate the standard deviation (SD) of triplicated measurements, periods without measurement are  
 591 linearly interpolated.

592

(a) hyponitrous acid pathway



(b) nitramide pathway

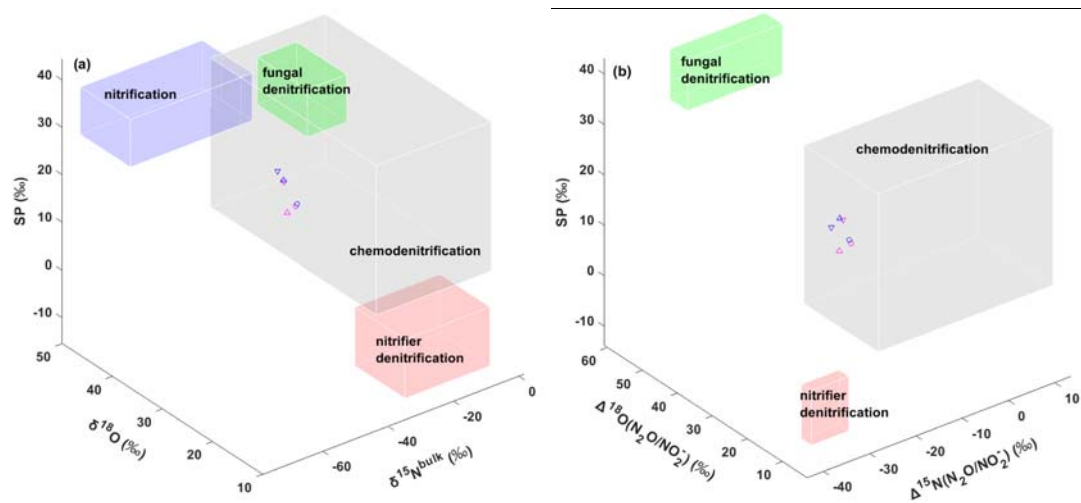


593

594 **Fig. 6.** Proposed hyponitrous acid pathway (a) and nitramide pathway (b) of  $\text{N}_2\text{O}$  formation in the  
 595 reactions of  $\text{NO}_2^-$  with lignin derivatives. The reaction of  $\text{NO}_2^-$  with 4-hydroxybenzoic acid is taken as  
 596 an example.

597

598  
599



600  
601  
602  
603  
604  
605

**Fig. 7.** Three dimensional end-member maps of N<sub>2</sub>O isotopic signatures (a), and SP<sub>N<sub>2</sub>O</sub> and net <sup>15</sup>N and <sup>18</sup>O isotopic effects (b). Pink and blue symbols represent mean values for unsterilized and sterilized soil samples, respectively. Downward triangles, agricultural soil samples; upward triangles, grassland soil samples; circles, forest soil samples.

## ACKNOWLEDGEMENTS

This study was supported by the Chinese Scholarship Council (scholarship no. 201406890023), the German Federal Ministry of Education and Research (BMBF) within the frame of the INPLAMINT project (grant no. 031A561A) and the Swiss National Science Foundation (grant no. CRSII5\_170876). Jing Wei was supported by the EMPAPOSTDOCS-II programme, which received funding from the European Union's Horizon 2020 research and innovation programme under the Marie Skłodowska-Curie grant agreement number 754364. The authors would like to thank Steffen Rothardt and Henning Kage at the Christian-Albrechts-Universität zu Kiel (CAU) for providing the agricultural soil, Chang Liu and Jack Hensley for helping to develop the MATLAB code for data analysis, and Kristyna Kantnerova and Patrik Zanchetta for their technical support during the experiments.



617 **Supporting Information Available**

618

619 **Supporting Information.** Stepwise regression of N<sub>2</sub>O isotopocule ratios vs N<sub>2</sub>O concentration is  
620 included.

621 **Research Data.** Wei, Jing (2019), “Data for: First real-time isotopic characterization of N<sub>2</sub>O from  
622 chemodenitrification”, Mendeley Data, V1, doi: 10.17632/ntt24tgh2b.1.

623

## REFERENCES

- Austin A.T. (1961) Nitrosation in organic chemistry. *Sci. Prog.* **XLIX**, 619-640.
- Berns A.E., Philipp H., Narres H.D., Buraue P., Vereecken H. and Tappe W. (2008) Effect of gamma - sterilization and autoclaving on soil organic matter structure as studied by solid state NMR, UV and fluorescence spectroscopy. *Eur. J. Soil Sci.* **59**, 540-550.
- Bol R., Toyoda S., Yamulki S., Hawkins J.M.B., Cardenas L.M. and Yoshida N. (2003) Dual isotope and isotopomer ratios of N<sub>2</sub>O emitted from a temperate grassland soil after fertiliser application. *Rapid Commun. Mass Spectrom.* **17**, 2550-2556.
- Bringas M., Semelak J., Zeida A. and Estrin D.A. (2016) Theoretical investigation of the mechanism of nitroxyl decomposition in aqueous solution. *J. Inorg. Biochem.* **162**, 102-108.
- Caranto J.D. and Lancaster K.M. (2017) Nitric oxide is an obligate bacterial nitrification intermediate produced by hydroxylamine oxidoreductase. *Proc. Natl. Acad. Sci. U.S.A* **114**, 8217-8222.
- Chalk P.M. and Smith C.J. (1983) Chemodenitrification, in: *Gaseous loss of nitrogen from plant-soil systems* (eds. J.R. Freney, J.R. Simpson). Martinus Nijhoff, Hague.
- Decock C. and Six J. (2013) How reliable is the intramolecular distribution of <sup>15</sup>N in N<sub>2</sub>O to source partition N<sub>2</sub>O emitted from soil? *Soil Biol. Biochem.* **65**, 114-127.
- Fehling C. (2012) Mechanistic insights from the <sup>15</sup>N-site preference of nitrous oxide utilizing high resolution near-infrared cw cavity ringdown spectroscopy and density functional theory calculations. Ph. D. thesis, Kiel University.
- Fehling C. and Friedrichs G. (2011) Dimerization of HNO in aqueous solution: an interplay of solvation effects, fast acid-base equilibria, and intramolecular hydrogen bonding? *J. Am. Chem. Soc.* **133**, 17912-17922.
- Frame C.H. and Casciotti K.L. (2010) Biogeochemical controls and isotopic signatures of nitrous oxide production by a marine ammonia-oxidizing bacterium. *Biogeosciences* **7**, 2695-2709.

648 Grabb K.C., Buchwald C., Hansel C.M. and Wankel S.D. (2017) A dual nitrite isotopic investigation of  
649 chemodenitrification by mineral-associated Fe(II) and its production of nitrous oxide.  
650 *Geochim. Cosmochim. Acta* **196**, 388-402.

651 Gröning M. (2018) TEL Technical Note No. 01: SICalib User Manual (Stable Isotope Calibration for  
652 routine  $\delta$ -scale measurements) Ver 2.16j. *International Atomic Energy Agency*, Vienna,  
653 Austria.

654 Harris E., Joss A., Emmenegger L., Kipf M., Wolf B., Mohn J. and Wunderlin P. (2015) Isotopic  
655 evidence for nitrous oxide production pathways in a partial nitrification-anammox reactor.  
656 *Water Res.* **83**, 258-270.

657 Heil J., Wolf B., Brüggemann N., Emmenegger L., Tuzson B., Vereecken H. and Mohn J. (2014) Site-  
658 specific  $^{15}\text{N}$  isotopic signatures of abiotically produced  $\text{N}_2\text{O}$ . *Geochim. Cosmochim. Acta* **139**,  
659 72-82.

660 Heil J., Liu S., Vereecken H. and Brüggemann N. (2015) Abiotic nitrous oxide production from  
661 hydroxylamine in soils and their dependence on soil properties. *Soil Biol. Biochem.* **84**, 107-  
662 115.

663 Ibraim E., Harris E., Eyer S., Tuzson B., Emmenegger L., Six J. and Mohn J. (2018) Development of a  
664 field-deployable method for simultaneous, real-time measurements of the four most  
665 abundant  $\text{N}_2\text{O}$  isotopocules. *Isotopes Environ. Health Stud.* **54**, 1-15.

666 IPCC (2013) Climate change 2013: The physical science basis. Contribution of working group I to the  
667 fifth assessment report of the intergovernmental panel on climate change. Cambridge  
668 University Press, Cambridge, United Kingdom and New York, NY, USA.

669 Jones L.C., Peters B., Pacheco J.S.L., Casciotti K.L. and Fendorf S. (2015) Stable isotopes and iron oxide  
670 mineral products as markers of chemodenitrification. *Environ. Sci. Technol.* **49**, 3444-3452.

671 Jung M.Y., Well R., Min D., Giesemann A., Park S.J., Kim J.G., Kim S.J. and Rhee S.K. (2014) Isotopic  
672 signatures of  $\text{N}_2\text{O}$  produced by ammonia-oxidizing archaea from soils. *ISME J.* **8**, 1115-1125.

673 Kainz G. and Huber H. (1959) Zur Kenntnis der Reaktionen, die bei der Aminostickstoffbestimmung  
 674 anomale Resultate verursachen. Die Anomalie der Isonitrosoverbindungen. *Microchim. Acta*  
 675 **47**, 337-345.

676 Kaiser K. and Benner R. (2012) Characterization of lignin by gas chromatography and mass  
 677 spectrometry using a simplified CuO oxidation method. *Anal. Chem.* **84**, 459-464.

678 Kool D.M., Wrage N., Oenema O., Dolfig J. and Van Groenigen J.W. (2007) Oxygen exchange  
 679 between (de)nitrification intermediates and H<sub>2</sub>O and its implications for source  
 680 determination of NO<sub>3</sub><sup>-</sup> and N<sub>2</sub>O: a review. *Rapid Commun. Mass Spectrom.* **21**, 3569-3578.

681 Kool D.M., Wrage N., Oenema O., Harris D. and Van Groenigen J.W. (2009) The <sup>18</sup>O signature of  
 682 biogenic nitrous oxide is determined by O exchange with water. *Rapid Commun. Mass*  
 683 *Spectrom.* **23**, 104-108.

684 Kool D.M., Wrage N., Oenema O., Van Kessel C. and Van Groenigen J.W. (2011) Oxygen exchange  
 685 with water alters the oxygen isotopic signature of nitrate in soil ecosystems. *Soil Biol.*  
 686 *Biochem.* **43**, 1180-1185.

687 Lewicka-Szczebak D., Augustin J., Giesemann A. and Well R. (2017) Quantifying N<sub>2</sub>O reduction to N<sub>2</sub>  
 688 based on N<sub>2</sub>O isotopocules – validation with independent methods (helium incubation and  
 689 <sup>15</sup>N gas flux method). *Biogeosciences* **13**, 711-732.

690 Lewicka-Szczebak D., Dyckmans J., Kaiser J., Marca A., Augustin J. and Well R. (2016) Oxygen isotope  
 691 fractionation during N<sub>2</sub>O production by soil denitrification. *Biogeosciences* **13**, 1129-1144.

692 Liu S., Han P., Hink L., Prosser J.I., Wagner M. and Brüggemann N. (2017) Abiotic conversion of  
 693 extracellular NH<sub>2</sub>OH contributes to N<sub>2</sub>O emission during ammonia oxidation. *Environ. Sci.*  
 694 *Technol.* **51**, 13122-13132.

695 Maharjan B. and Venterea R.T. (2013) Nitrite intensity explains N management effects on N<sub>2</sub>O  
 696 emissions in maize. *Soil Biol. Biochem.* **66**, 229-238.

697 Mandernack K., Mills, Johnson C. and Rahn T. (2009) The δ<sup>15</sup>N and δ<sup>18</sup>O values of N<sub>2</sub>O produced  
 698 during the co-oxidation of ammonia by methanotrophic bacteria. *Chem. Geol.* **267**, 96-107.

699 Mohn J., Wolf B., Toyoda S., Lin C.T., Liang M.C., Bruggemann N., Wissel H., Steiker A.E., Dyckmans J.,  
700 Szvec L., Ostrom N.E., Casciotti K.L., Forbes M., Gieseemann A., Well R., Doucett R.R., Yarnes  
701 C.T., Ridley A.R., Kaiser J. and Yoshida N. (2014) Interlaboratory assessment of nitrous oxide  
702 isotopomer analysis by isotope ratio mass spectrometry and laser spectroscopy: current  
703 status and perspectives. *Rapid Commun. Mass Spectrom.* **28**, 1893-1903.

704 Obayashi E., Takahashi S. and Shiro Y. (1998) Electronic structure of reaction intermediate of  
705 cytochrome P450nor in its nitric oxide reduction. *J. Am. Chem. Soc.* **120**, 12964-12965.

706 Ostrom N.E., Gandhi H., Trubl G. and Murray A.E. (2016) Chemodenitrification in the cryoecosystem  
707 of Lake Vida, Victoria Valley, Antarctica. *Geobiology* **14**, 575-587.

708 Ostrom N.E., Pitt A., Sutka R., Ostrom P.H., Grandy A.S., Huizinga K.M. and Robertson G.P. (2007)  
709 Isotopologue effects during N<sub>2</sub>O reduction in soils and in pure cultures of denitrifiers. *J.*  
710 *Geophys. Res. Biogeosci.* **112**, G02005.

711 Peters B., Casciotti K.L., Samarkin V.A., Madigan M.T., Schutte C.A. and Joye S.B. (2014) Stable  
712 isotope analyses of NO<sub>2</sub><sup>-</sup>, NO<sub>3</sub><sup>-</sup>, and N<sub>2</sub>O in the hypersaline ponds and soils of the McMurdo  
713 Dry Valleys, Antarctica. *Geochim. Cosmochim. Acta* **135**, 87-101.

714 Ravishankara A.R., Daniel J.S. and Portmann R.W. (2009) Nitrous oxide (N<sub>2</sub>O): the dominant ozone-  
715 depleting substance emitted in the 21st century. *Science* **326**, 123-125.

716 Röckmann T. and Levin I. (2005) High-precision determination of the changing isotopic composition  
717 of atmospheric N<sub>2</sub>O from 1990 to 2002. *J. Geophys. Res.* **110**, D21304.

718 Rohe L., Anderson T.H., Braker G., Flessa H., Gieseemann A., Lewicka-Szczebak D., Wrage-Mönnig N.  
719 and Well R. (2014) Dual isotope and isotopomer signatures of nitrous oxide from fungal  
720 denitrification – a pure culture study. *Rapid Commun. Mass Spectrom.* **28**, 1893-1903.

721 Rohe L., Well R. and Lewicka-Szczebak D. (2017) Use of oxygen isotopes to differentiate between  
722 nitrous oxide produced by fungi or bacteria during denitrification. *Rapid Commun. Mass*  
723 *Spectrom.* **31**, 1297-1312.

724 Samarkin V.A., Madigan M.T., Bowles M.W., Casciotti K.L., Priscu J.C., McKay C.P. and Joye S.B. (2010)  
725 Abiotic nitrous oxide emission from the hypersaline Don Juan Pond in Antarctica. *Nat. Geosci.*  
726 **3**, 341-344.

727 Santoro A.E., Buchwald C., McIlvin M.R. and Casciotti K.L. (2011) Isotopic signature of N<sub>2</sub>O produced  
728 by marine ammonia-oxidizing archaea. *Science* **333**, 1282-1285.

729 Snider D.M., Schiff S.L. and Spoelstra J. (2009) <sup>15</sup>N/<sup>14</sup>N and <sup>18</sup>O/<sup>16</sup>O stable isotope ratios of nitrous  
730 oxide produced during denitrification in temperate forest soils. *Geochim. Cosmochim. Acta*  
731 **73**, 877-888.

732 Snider D.M., Venkiteswaran J.J., Schiff S.L. and Spoelstra J. (2015) From the ground up: Global nitrous  
733 oxide sources are constrained by stable isotope values. *PLoS ONE* **10**, e0118954.

734 Stein L.Y. (2011) Surveying N<sub>2</sub>O producing pathways in bacteria. *Methods Enzymol.* **486**, 131-152.

735 Stevenson F.J. and Swaby R.J. (1964) Nitrosation of soil organic matter: I. Nature of gases evolved  
736 during nitrous acid treatment of lignins and humic substances. *Soil Sci. Soc. Am. J.* **28**, 773-  
737 778.

738 Sutka R.L., Adams G.C., Ostrom N.E. and Ostrom P.H. (2008) Isotopologue fractionation during N<sub>2</sub>O  
739 production by fungal denitrification. *Rapid Commun. Mass Spectrom.* **22**, 3989-3996.

740 Sutka R.L., Ostrom N.E., Ostrom P.H., Breznak J.A., Gandhi H., Pitt A.J. and Li F. (2006) Distinguishing  
741 nitrous oxide production from nitrification and denitrification on the basis of isotopomer  
742 abundances. *Appl. Environ. Microbiol.* **72**, 638-644.

743 Sutka R.L., Ostrom N.E., Ostrom P.H., Gandhi H. and Breznak J.A. (2003) Nitrogen isotopomer site  
744 preference of N<sub>2</sub>O produced by *Nitrosomonas europaea* and *Methylococcus capsulatus* Bath.  
745 *Rapid Commun. Mass Spectrom.* **17**, 738-745.

746 Thevenot M., Dignac M.F. and Rumpel C. (2010) Fate of lignins in soils: A review. *Soil Biol. Biochem.*  
747 **42**, 1200-1211.

748 Toyoda S., Iwai H., Koba K. and Yoshida N. (2009) Isotopomeric analysis of N<sub>2</sub>O dissolved in a river in  
749 the Tokyo metropolitan area. *Rapid Commun. Mass Spectrom.* **23**, 809-821.

750 Toyoda S., Kuroki N., Yoshida N., Ishijima K., Tohjima Y. and Machida T. (2013) Decadal time series of  
 751 tropospheric abundance of N<sub>2</sub>O isotopomers and isotopologues in the Northern Hemi-sphere  
 752 obtained by the long-term observation at Hateruma Island, Japan. *J. Geophys. Res.* **118**, 3369-  
 753 3381.

754 Toyoda S., Mutoke H., Yamagishi H., Yoshida N. and Tanji Y. (2005) Fractionation of N<sub>2</sub>O isotopomers  
 755 during production by denitrifier. *Soil Biol. Biochem.* **37**, 1535-1545.

756 Toyoda S., Yano M., Nishimura S.-i., Akiyama H., Hayakawa A., Koba K., Sudo S., Yagi K., Makabe A.,  
 757 Tobari Y., Ogawa N.O., Ohkouchi N., Yamada K. and Yoshida N. (2011) Characterization and  
 758 production and consumption processes of N<sub>2</sub>O emitted from temperate agricultural soils  
 759 determined via isotopomer ratio analysis. *Global Biogeochem. Cy.* **25**, GB2008.

760 Toyoda S. and Yoshida N. (1999) Determination of nitrogen isotopomers of nitrous oxide on a  
 761 modified isotope ratio mass spectrometer. *Anal. Chem.* **71**, 4711-4718.

762 Toyoda S., Yoshida N., Miwa T., Matsui Y., Yamagishi H., Tsunogai U., Nojiri Y. and Tsurushima N.  
 763 (2002) Production mechanism and global budget of N<sub>2</sub>O inferred from its isotopomers in the  
 764 western North Pacific. *Geophys. Res. Lett.* **29**, 7-1-7-4.

765 Venterea R.T. (2007) Nitrite-driven nitrous oxide production under aerobic soil conditions: kinetics  
 766 and biochemical controls. *Global Change Biol.* **13**, 1798-1809.

767 Waechter H., Mohn J., Tuzson B., Emmenegger L. and Sigrist M.W. (2008) Determination of N<sub>2</sub>O  
 768 isotopomers with quantum cascade laser based absorption spectroscopy. *Opt. Express* **16**,  
 769 9239-9244.

770 Wankel S.D., Ziebis W., Buchwald C., Charoenpong C., de Beer D., Dentinger J., Xu Z. and Zengler K.  
 771 (2017) Evidence for fungal and chemodenitrification based N<sub>2</sub>O flux from nitrogen impacted  
 772 coastal sediments. *Nat. Commun.* **8**, 15595.

773 Watmough N.J., Field S.J., Hughes R.J. and Richardson D.J. (2009) The bacterial respiratory nitric  
 774 oxide reductase. *Biochem. Soc. Trans.* **37**, 392-399.

775 Wei J., Amelung W., Lehndorff E., Schloter M., Vereecken H. and Brüggemann N. (2017a) N<sub>2</sub>O and  
776 NO<sub>x</sub> emissions by reactions of nitrite with soil organic matter of a Norway spruce forest.  
777 *Biogeochemistry* **132**, 1-18.

778 Wei J., Zhou M., Vereecken H. and Brüggemann N. (2017b) Large variability of CO<sub>2</sub> and N<sub>2</sub>O emissions  
779 and of <sup>15</sup>N site preference of N<sub>2</sub>O from reactions of nitrite with lignin and its derivatives at  
780 different pH. *Rapid Commun. Mass Spectrom.* **31**, 1333-1343.

781 Werle P., Mucke R. and Slemr F. (1993) The limits of signal averaging in atmospheric trace-gas  
782 monitoring by tunable diode-laser absorption-spectroscopy (TDLAS). *Appl. Phys. B* **57**, 131-  
783 139.

784 WMO (2016) WMO Greenhouse Gas Bulletin: The state of greenhouse gases in the atmosphere  
785 based on global observations through 2015. World Meteorological Organization, Geneva.

786 Wolf B., Merbold L., Decock C., Tuzson B., Harris E., Six J., Emmenegger L. and Mohn J. (2015) First  
787 on-line isotopic characterization of N<sub>2</sub>O above intensively managed grassland. *Biogeosciences*  
788 **12**, 2517-2531.

789 Wunderlin P., Lehmann M.F., Siegrist H., Tuzson B., Joss A., Emmenegger L. and Mohn J. (2013)  
790 Isotope signatures of N<sub>2</sub>O in a mixed microbial population system: Constraints on N<sub>2</sub>O  
791 producing pathways in wastewater treatment. *Environ. Sci. Technol.* **47**, 1339-1348.

792 Yamazaki T., Hozuki T., Arai K., Toyoda S., Koba K., Fujiwara T. and Yoshida N. (2014) Isotopomeric  
793 characterization of nitrous oxide produced by reaction of enzymes extracted from nitrifying  
794 and denitrifying bacteria. *Biogeosciences* **11**, 2679-2689.

795 Yoshida N. (1988) <sup>15</sup>N-depleted N<sub>2</sub>O as a product of nitrification. *Nature* **335**, 528-529.

796 Zacharias S., Bogen H., Samaniego L., Mauder M., Fuß R., Pütz T., Frenzel M., Schwank M., Baessler  
797 C., Butterbach-Bahl K., Bens O., Borg E., Brauer A., Dietrich P., Hajnsek I., Helle G., Kiese R.,  
798 Kunstmann H., Klotz S., Munch J.C., Papen H., Priesack E., Schmid H.P., Steinbrecher R.,  
799 Rosenbaum U., Teutsch G. and Vereecken H. (2011) A Network of Terrestrial Environmental  
800 Observatories in Germany. *Vadose Zone J.* **10**, 955-973.



801 Zhang W., Li Y., Xu C., Li Q. and Lin W. (2016) Isotope signatures of N<sub>2</sub>O emitted from vegetable soil:  
802 Ammonia oxidation drives N<sub>2</sub>O production in NH<sub>4</sub><sup>+</sup>-fertilized soil of North China. *Sci. Rep.* **6**,  
803 29257.

804 Zhu-Barker X., Cavazos A.R., Ostrom N.E., Horwath W.R. and Glass J.B. (2015) The importance of  
805 abiotic reactions for nitrous oxide production. *Biogeochemistry* **126**, 251-267.

806 Zou Y., Hirono Y., Yanai Y., Hattori S., Toyoda S. and Yoshida N. (2014) Isotopomer analysis of nitrous  
807 oxide accumulated in soil cultivated with tea (*Camellia sinensis*) in Shizuoka, central Japan.  
808 *Soil Biol. Biochem.* **77**, 276-291.